Chem Soc Rev

REVIEW ARTICLE

View Article Online
View Journal | View Issue

Cite this: *Chem. Soc. Rev.*, 2025, **54**, 4391

Self-healing behavior of superhard covalent bond materials

Keliang Qiu,†[a] Xiang Li,†[a] Yanhong Li,[a] Yonghai Yue*[ab] and Lin Guo *[a]

In recent years, superhard covalently bonded materials have drawn a great deal of attention due to their excellent mechanical properties and potential applications in various fields. This review focuses on the self-healing behavior of these materials, outlining state-of-the-art research results. In detail, we discuss current self-healing mechanisms of self-healing materials including extrinsic healing mechanisms (such as microencapsulation, oxidative healing, shape memory, *etc.*) and intrinsic healing (dynamic covalent bonding, supramolecular interactions, diffusion, defect-driven processes, *etc.*). We also provide an overview of the progress in the self-healing behavior of superhard covalently bonded materials and the mechanisms of permanent covalent bonding healing. Additionally, we analyze the factors that influence the healing properties of these materials. Finally, the main findings and an outlook on the future directions and challenges of this emerging field are summarized in the Conclusion section.

Received 24th November 2024

DOI: 10.1039/d4cs01182a

rsc.li/chem-soc-rev

1. Introduction

Drawing inspiration from nature is a crucial strategy for developing new materials.[1–5] Over billions of years of natural selection, biological organisms have evolved unique damage repair mechanisms, which is an essential survival feature of life forms. For instance, small wounds on human skin can heal after a sufficient period of time, as fractures can be gradually repaired. Even plants have a greater capacity for self-repair or regeneration compared to animals. In contrast, man-made materials often fail catastrophically due to natural or anthropogenic degradation or degradation over time, resulting in the formation of micro-cracks.[6–8] Therefore, in order to improve the safety, reliability and service life of the materials, researchers have mimicked the self-healing properties of living organisms for applications in aerospace, energy, and biomedicine.[9–13]

Currently, research on self-healing materials is only a few decades old. Their self-healing mechanisms have not yet attained the complexity found in the physical events and chemical reactions involved in the self-healing process of living systems. Nevertheless, significant progress has been made in the study of self-healing materials, mainly in the field of polymeric materials, which are generally soft and deformable and more likely to exhibit self-healing properties.[14–16] In addition, some research progress have been made in self-healing metallic materials and self-healing

[a] *School of Chemistry, Beihang University, Beijing, China. E-mail: yueyonghai@buaa.edu.cn, guolin@buaa.edu.cn*
[b] *State Key Laboratory of Silicate Materials for Architectures, Wuhan University of Technology, Wuhan, China*
† These authors contributed equally to this work.

Keliang Qiu

Keliang Qiu received his PhD from Beihang University under the supervision of Prof. Yonghai Yue. He is currently a postdoctoral researcher at Beihang University, focusing on multi-scale, multi-field coupled in situ studies of the structure–property relationships in structural materials.

Xiang Li

Xiang Li is a PhD student at Beihang University under the supervision of Professor Yue Yonghai. Xiang Li is dedicated to the study of failure mechanisms of mechanical behaviour of metallic materials under different external fields at the micro and nano scales.

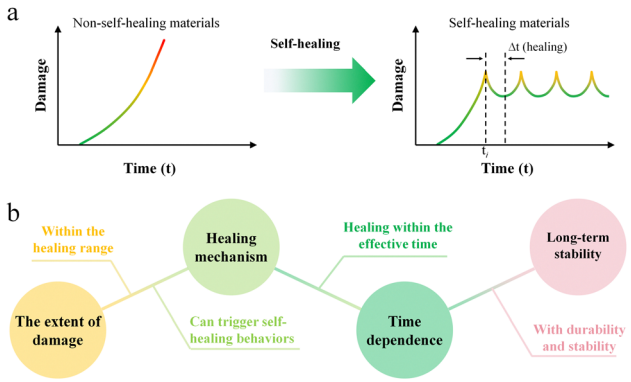

Fig. 1 Diagram of self-healing material properties. (a) Diagram of relationship between damage and time of non-self-healing and self-healing materials. (b) The main factors affecting self-healing materials.

ceramic materials likewise.[17,18] In contrast, Research on self-healing superhard covalent materials remains preliminary and exploratory.

1.1 What is self-healing?

So, what is self-healing? Over time, the degradation of synthetic materials can cause damage or micro cracks, reducing the material's safety and reliability, potentially resulting in catastrophic failure within its effective service life.[19,20] Therefore, "Removing" damage through damage management is an important solution, that explores the ability of materials to recover from physical damage, inspired by the self-healing capabilities of living organisms. The ability of materials to automatically and autonomously heal or repair damage without any external intervention is defined as self-healing.[21] Once the self-healing behavior is triggered, the tendency of non-self-healing materials to progressively accumulate damage over time until failure ($d(\text{damage})/dt \geq 0 (0 < t <$ life time)) shifts to that of self-healing materials, which cyclically remove damage ($d(\text{damage})/dt < 0 (t_i < t < t_{i+\Delta t(\text{healing})})$) to ensure sustainable service (Fig. 1a). The healing of material mechanical properties is paramount, as mechanical performance underpins the practical applications of materials. Once physical failures such as collapse and fracture occur in materials, they will directly trigger catastrophic failures. Therefore, in order to more accurately describe the self-healing ability of materials, the ratio of the healed stress (or strength) to the initial stress (or strength) is usually defined as the healing efficiency. Artificial self-healing materials can be divided into two categories based on whether their self-healing behavior needs to be triggered by the external environment: one category is active, *i.e.*, it does not need to be triggered by the external environment to achieve active repair;[22–26] the other category requires external intervention to trigger self-healing behavior.[27–30]

It is important to ensure that the self-healing function of the material is realized, so the following aspects need to be fully understood (Fig. 1b): (1) the extent of damage. To clarify the location and scale of the damage of the material, it should be within the scope of the material's repairable capacity; (2) healing mechanism. Give full play to the self-healing ability of the material and improve the healing efficiency; (3) time dependence. Self-healing is not instantaneous but takes a certain amount of time, so the healing time should be reduced as much as possible; (4) long-term stability. This self-healing ability can remain effective until the material completely fails, allowing for multiple healing cycles. In addition, other factors must be considered, such as ensuring that the material's performance is not significantly reduced after healing, biocompatibility (biomaterials) and so on.

1.2 Types of self-healing materials

The self-healing phenomenon in non-living materials was discovered long ago, for example, mica in nature can heal itself after fracture.[31,32] In addition, self-healing phenomena similar to biological self-healing have likewise been found in man-made materials, such as cements, polymer materials, and so on, which have been widely noticed.[33–36] With the continuous research on self-healing materials, two main types of self-healing materials have been developed, *i.e.*, extrinsic self-healing[37–39] and intrinsic self-healing.[40–42] Extrinsic self-healing refers to achieving self-healing by adding non matrix healing agents.[43] Intrinsic self-healing

Yonghai Yue

Yonghai Yue is a professor at the School of Chemistry, Beihang University. He received his PhD degree from the Institute of Microstructure and Properties of Advanced Materials, Beijing University of Technology in 2012. He was a visiting scholar at Arizona State University in 2014. His research area focuses on the design and preparation of lightweight and high-strength materials, the exploration of multi-field coupled in situ microscopic failure mechanisms and the exploration of potential applications.

Lin Guo

Guo Lin is a full-time professor at the School of Chemistry, Beihang University. he received his PhD degree from the School of Chemical Engineering and Materials, Beijing Institute of Technology in 1997. He was a visiting scholar at the Hong Kong University of Science and Technology in 1999 and a Humboldt Scholar at the Dresden University of Technology. His research interests focus on the design and preparation of amorphous micro- and nanomaterials and the exploration of potential performance applications.

materials achieve damage repair relying on their own dynamic chemical bonding or their own physical properties. A variety of self-healing mechanisms have been developed for both types of self-healing materials.

1.3 Superhard covalently bonded materials

Superhard covalently bonded materials occupy a unique position within the broader spectrum of materials. These materials are mainly composed of covalent compounds. The covalent bonds within them are short and strong, endowing them with excellent resistance to elastic and plastic deformation. Generally, the (Vickers) hardness value of superhard materials exceeds 40 GPa, often far exceeding that of traditional metal materials and ordinary ceramic materials. Thanks to their exceptional hardness, superhard covalent bond materials exhibit remarkable wear resistance, making them highly effective in applications such as cutting tools, abrasives, and grinding tools. Furthermore, superhard materials typically showcase a range of other distinctive properties such as high compressive strength, remarkable shear resistance, a high bulk modulus, a high melting point, chemical inertness, and excellent thermal conductivity.[44] These attributes further enhance their versatility and performance in demanding industrial applications.

However, superhard materials are among the rarest of functional inorganic solids, representing less than 0.1% of the entire material system.[45] Currently, the prevalent and commercially accessible superhard materials are predominantly diamond and cubic boron nitride. Over the past few decades, considerable efforts have been made to develop superhard materials that surpass the hardness and performance of cubic boron nitride and diamond. To this end, both quantitative hardness prediction techniques and experimental approaches have been advanced, aimed at significantly improving the properties of existing superhard materials.[46,47] In addition, researchers design and discover novel superhard materials experimentally and theoretically by combining light elements like boron, carbon, nitrogen, and/or oxygen to form short covalent bonds or introducing elements with extremely high valence electron density.[48] At present, the hardness of synthetic diamond blocks has been increased to 276 GPa.[49] The hardness of cubic boron nitride has also exceeded 100 GPa.[50] Even the hardness of silicon carbide has surpassed 40 GPa.[51] However, in practical applications, superhard covalent bond materials are not without flaws. For example, diamond has serious limitations that severely restrict its industrial applications in the processing of ferrous metal materials: it has poor thermal stability and high chemical reactivity with ferroalloys. As for cubic boron nitride, although it is suitable for the processing of ferrous metal materials, the hardness and toughness of its single crystal are only half of those of single crystal diamond.[52] It is important to note that when superhard covalent-bonded materials are exposed to demanding operational conditions—such as sustained mechanical stress, thermal cycling, and chemical corrosion—various forms of damage, including microcracks and other defects, inevitably develop within the materials. These defects continuously expand and accumulate during service, and ultimately are highly likely to trigger the catastrophic failure of the materials, posing serious potential threats to the safe operation of related engineering equipment.

Therefore, once the self-healing of superhard covalent bond materials is achieved, it will greatly expand their application scope, significantly enhance their service performance under extreme environments, and thus bring about a new revolution in the field of materials science and engineering. In view of this, in order to develop superhard covalent bond self-healing materials more effectively and provide guidance for the development of other self-healing materials, we have provided a comprehensive overview of the primary self-healing mechanisms currently in use. We have also highlighted the present state of development in self-healing superhard covalent-bond materials and, ultimately, outlined prospective directions for future advancements.

2. Mechanisms of self-healing

2.1 Extrinsic self-healing mechanisms

Extrinsic self-healing mechanism is an important branch in the study of self-healing materials, which refers to the self-healing of materials by externally-added restorative agents after damage.

2.1.1 Microencapsulation embedment. For the study of extrinsic self-healing mechanisms, the microencapsulation embedment design scheme is an important breakthrough. In 2001, White *et al.* developed the first structural polymeric material with the ability to autonomically repair cracks (Fig. 2a), marking a new stage in the development of self-healing materials.[37] The design of this self-healing material is achieved by compounding microcapsules containing healing agents with an epoxy resin matrix rich in catalysts, and the stiffness of the capsule has an effect on the crack extension path (Fig. 2b). When microcracks form in the material, they cause the microcapsules to rupture, resulting in the automatic release of the healing agent, which polymerizes and converts to a solid phase in the presence of a catalyst within the matrix. This process bonds the cracked surfaces and achieves a healing efficiency of up to 75%. This healing mechanism occurs autonomously. However, this microencapsulation embedment design allows for healing only at a given location, and the number of healing sessions is closely related to the amount of healing agent in the localized area, so once the healing agent is depleted the location can no longer heal itself. Inspired by vascular networks in biological systems that deliver essential components for healing, a self-healing material with the three-dimensional vascular network structure (Fig. 2c and d) has been developed.[53] When a crack occurs in this self-healing material, the healing agent inside the microchannel enters the crack by capillary action and autonomously bonds the crack in the presence of a catalyst. Compared to microencapsulated structures, this self-healing material allows the healing cycle to be repeated (Fig. 2e). However, once the catalyst is depleted or the healing agent in the network is used up, this results in a decrease in the healing efficiency or even a loss of healing properties. In addition, self-healing can also be achieved by adding suitable thermoplastic materials, nanoparticles, *etc.*[54,55]

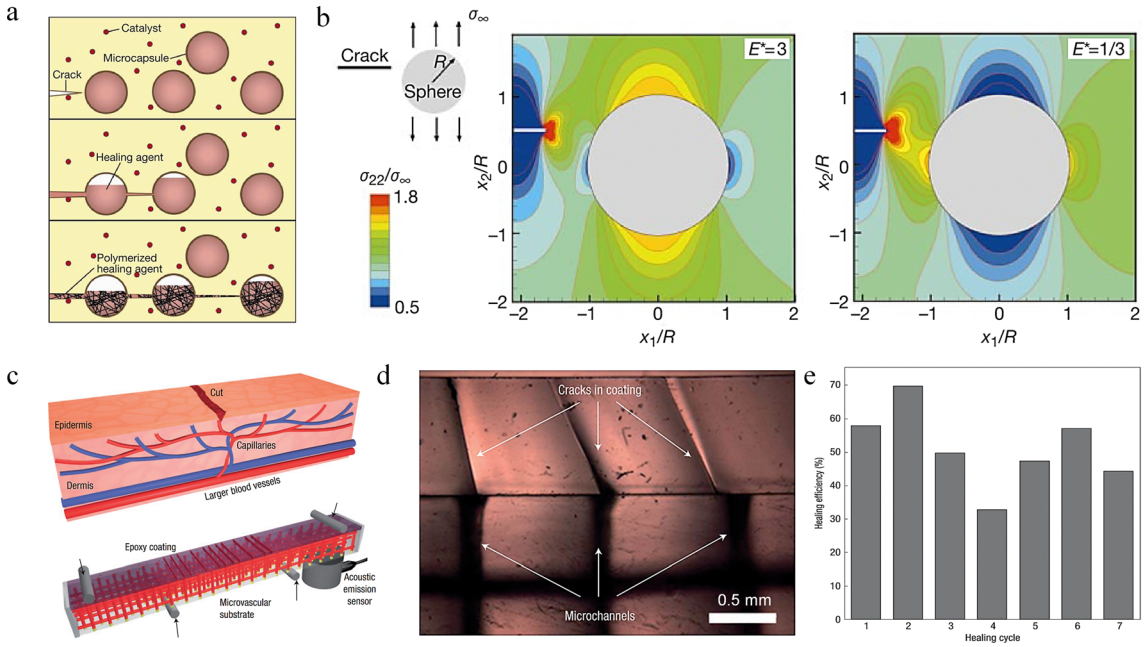

Fig. 2 Schematic of a typical extrinsic self-healing materials. (a) Schematic diagram of microencapsulated self-healing. (b) Analysis of the effect of relative stiffness of microcapsules on proximity crack extension paths.[37] Reproduced with permission from ref. 37, Copyright 2001, Springer Nature. (c) Schematic diagram of microvascular coating-substrate structure. (d) High-magnification cross-sectional image of the coating. (e) Healing efficiency for each successive loading.[53] Reproduced with permission from ref. 53, Copyright 2007, Springer Nature.

So far, in addition to polymer materials, a variety of self-healing materials based on extrinsic self-healing mechanisms have been developed in ceramics, metals and other materials. Mimicking the design of extrinsic self-healing mechanisms for polymers, self-healing can be achieved by embedding a capsule with a healing agent in the ceramic material. For example, the urea-formaldehyde microcapsules encapsulated with 1*H*,1*H*,2*H*,2*H*-perfluorodecyltriethoxysilane are homogeneously dispersed in a pure phosphate ceramic coating to obtain a phosphate ceramic coating with self-healing capability.[56] Self-healing metal composites can be designed by applying microencapsulation design strategies to embed low-melting-point metals into high-melting-point metals that act as healing agents.[57,58] Theoretically, this self-healing design model based on microcapsules demonstrates broad application potential and can endow the vast majority of materials with self-healing properties. However, in practical application scenarios, numerous factors have crucial impact on the initial mechanical properties of materials. These factors include the size and volume fraction of microcapsules, the interfacial bonding strength between microcapsules and the matrix, as well as the distribution state of microcapsules within the matrix. In matrix materials with relatively low mechanical properties, microcapsules may play a role in strengthening and toughening the material.

2.1.2 Oxidative healing mechanisms. For brittle materials such as ceramics, healing agent efflux can lead to the appearance of pores, resulting in reduced mechanical properties. This porosity is different from the diffusely distributed nanopores that enhance the mechanical properties of metals.[59] The current common mechanism for achieving self-healing of ceramic materials is the formation of oxides through high temperature oxidation reactions, known as an oxidative healing mechanism. This process effectively penetrates defects and flaws, promoting crack healing through volume expansion (Fig. 3a).[17,60–62] Binary carbides, nitrides, ternary MAX phases, and other materials typically act as a healing agent in ceramics. For example, Liu *et al.* added silicon carbide (SiC) whiskers and $TiSi_2$ particles as healing agents to alumina ceramics.[63] Cracks with several hundred micrometers long and 0.68 μm wide can be healed in high temperature (>800 °C) under air environments (high oxygen partial pressures) for 60 min. During this healing process, Ti_5Si_3 is preferentially oxidized, giving rise to TiO_2 and amorphous SiO_2. The *in situ* growth of TiO_2 leads to local crack bridging, while SiC oxidation results in the formation of liquid-phase SiO_2 intermediate oxidation states (Si_2O_3 and SiO), which compensates for the liquid-phase formation of Ti_5Si_3 to effectively fill the cracks (Fig. 3b). Flexural strength is fully restored after healing, which is due to the enormous volume expansion of TiO_2 and the strong adhesion between TiO_2 and Al_2O_3. Lin *et al.* investigated the crack healing behavior of ZrB_2-based ultrahigh-temperature ceramics reinforced with ZrO_2 fibers and SiC whiskers.[64] At a high oxidation temperature of 1200 °C for 30 min, both ZrB_2 and SiC were oxidized to form a dense oxide layer composed of ZrO_2 and SiO_2 to heal the cracks. The cracks with length of 7 μm and width of 5 μm in Ternary MAX phase Ti_3AlC_2 ceramics can be healed by formation of oxides (α-Al_2O_3 and rutile TiO_2) after treatment at high temperature (1100 °C) in an air environment for 2 h.[65]

Oxidative healing mechanisms can be triggered at high temperatures and high oxygen partial pressure environments (air environments), however, when oxygen partial pressure is

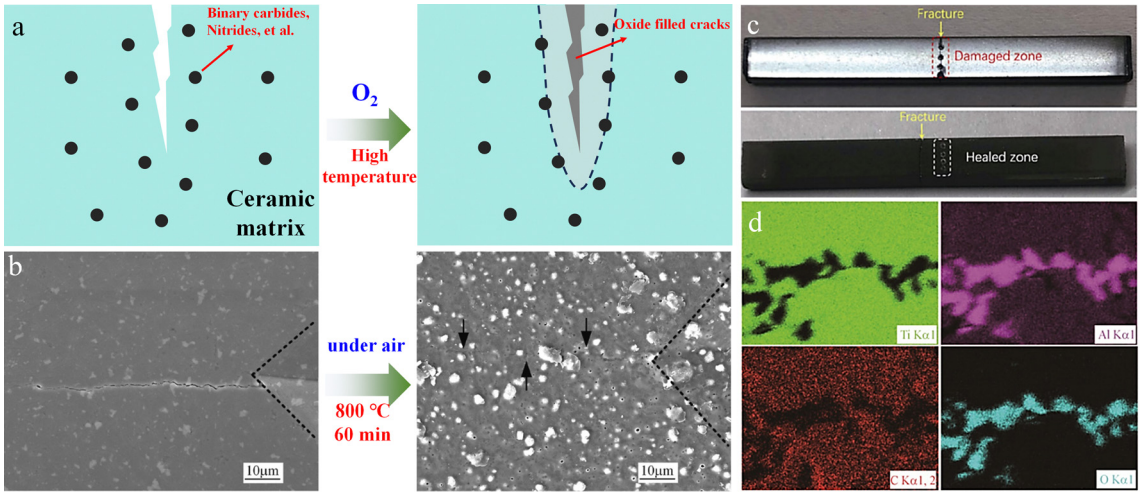

Fig. 3 Self-healing ceramics based on oxidizing mechanism. (a) Schematic of oxidative healing mechanisms. (b) Surface crack morphology of self-healing Al_2O_3 ceramic before and after healing.[63] Reproduced with permission from ref. 63, Copyright 2023, Elsevier. (c) and (d) Fracture behavior of Ti_2AlC before and after healing and EDS spectrum of the healed region.[66] Reproduced with permission from ref. 66, Copyright 2022, Springer Nature.

low, oxidative healing mechanisms are constrained and other healing mechanisms need to be considered. For example, Yao *et al.* found that Ti_2AlC exhibits a new mechanism of decomposition-induced crack healing at a low oxygen partial pressure of about 1 Pa, *i.e.*, microcracks are filled with decomposed TiC_x as the main phase.[66] The healed flexural strength exceeded the initial sample flexural strength after healing at 1400 °C for 2 h (Fig. 3c and d). From the energy dispersive spectrum (EDS) analysis, it can be seen that the Al_2O_3 grains fill the pores in the TiCx layer, resulting in a relatively dense healing zone. In low oxygen partial pressure environments of 5 Pa, another mechanism is the precipitation-induced crack healing mechanism, such as Sn-precipitation-induced crack healing in Ti_2SnC.[67]

2.1.3 Shape memory assisted healing. The shape memory effect refers to the ability of certain materials to return to their original shape under specific conditions (*e.g.* heat, light, *etc.*) after being changed, and common materials include shape memory alloys (SMA) and shape memory polymers (SMP). Instances of shape-memory-assisted healing are prevalent in nature; for example, when a leaf undergoes a transverse cut, it bends until healing occurs. Therefore, self-healing composites can be designed by introducing shape memory materials into the matrix. When damaged, these materials can recover their initial geometry by triggering the shape memory effect and thus achieve self-healing. An important advantage of the shape memory-assisted self-healing strategy is that, following the occurrence of a crack or fracture occurs in a material, it can self-heal by triggering the shape memory effect, allowing the material to actively close the crack while recovering its original shape. The most commonly used SMA materials are NiTi alloys, which have macroscopic shape reversibility due to the thermoelastic martensitic phase transition *i.e.* shape memory effect and superelastic effect.[68] By employing NiTi SMA wires to reinforce metallic materials, when a fracture occurs, the gap of the crack can be reduced or the fracture can be closed by heating.[69,70] Incorporating shape memory alloys (SMA) or supplementing them with shape memory polymers (SMP) in the matrix enhances self-healing performance by activating a shape memory response that restores the geometry and closes the crack upon damage.[71–74] Fisher *et al.* reinforced the aluminium-based matrix with a continuous NiTi SMA as the reinforcing phase.[75] When it fractured, the NiTi SMA deformed and bridged the two fractured ends. Healing at 592 °C for 24 h closes the crack using the contraction force generated by the NiTi SMA returning to its original shape, while the high temperature during healing leads to the softening and liquefaction of the eutectic micro components of the matrix which in turn fully fills the crack and achieves strength recovery (Fig. 4a and b). Shi *et al.* designed a set of polypropylene glycol (PPG)-MPU_x-PA_{1-x} with different ratios of 4,4′-methylenebisphenyl urea [MPU] (strong dynamic bonds) and *p*-phenylenediamine [PA] (weak dynamic bonds) to form strain-induced supramolecular nanostructures, which resulted in high energy density-enhanced SMPs that could enable centimeter-scale repair of puncture damage (Fig. 4c).[74] And it has the same performance before and after healing (Fig. 4d).

Shape memory-assisted self-healing methods have demonstrated effectiveness in promoting fracture closure; however, they generally require external conditions for activation. Hornatet *et al.* developed self-healing thermoplastic polyurethane (TPU) fibers and films assisted by autonomous shape memory under environmental conditions.[76] The efficient storage and release of conformational entropy during damage and repair is achieved through shape memory effects and utilises surface energy/tension to drive the repair process, with lower molecular weight TPU (MW ≈ 32 kDa) requires more time to self-repair through a distinct mechanism driven by surface/surface energy (Fig. 4f). Higher molecular weight TPU (MW ≈ 72 kDa) heal faster and mechanical properties are fully restored (Fig. 4e).

The realization of extrinsic healing in materials *via* the incorporation of embedded microcapsules, 3D vascular networks, oxidative healing mechanism components, and shape

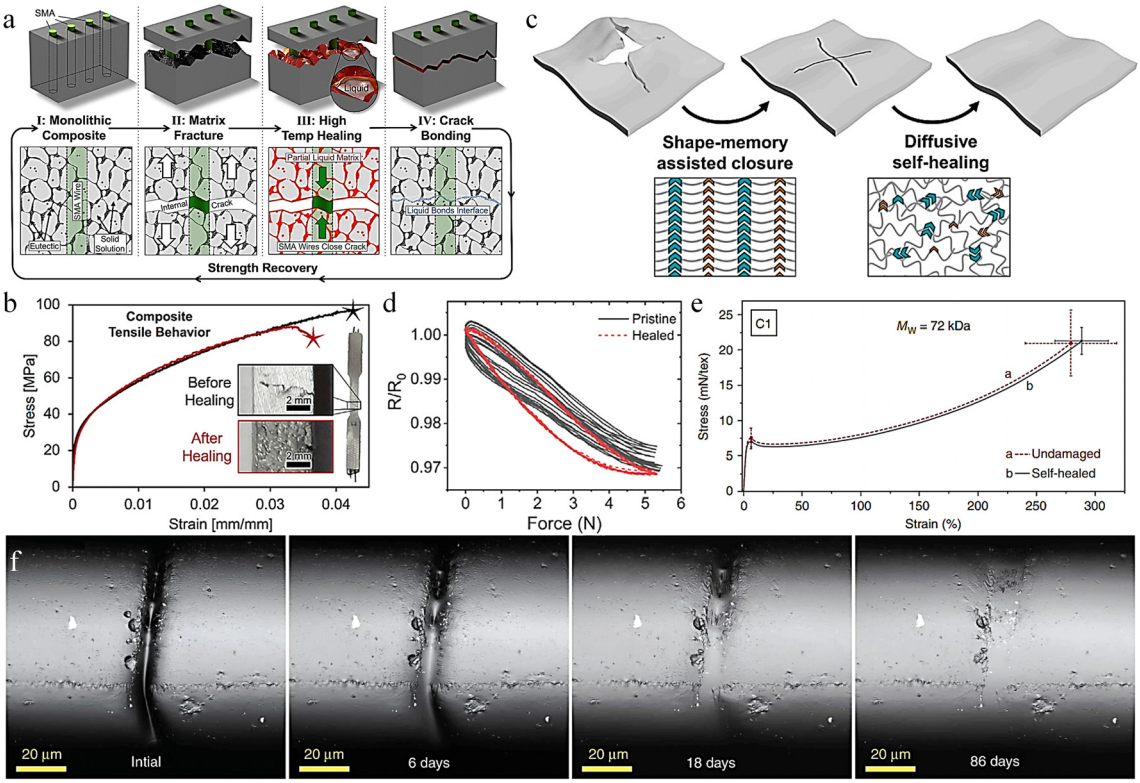

Fig. 4 Shape memory assists self-healing. (a) and (b) Healing process and mechanical properties of Al-3Si/SMA composites before and after healing.[75] Reproduced with permission from ref. 66, Copyright 2018, Elsevier. (c) and (d) Schematic of SMP-assisted self-healing and mechanical properties of PPG-$MPU_{0.7}$-$PA_{0.3}$ before and after healing.[74] Reproduced with permission from ref. 74, Copyright 2024, Elsevier. (e) and (f) Mechanical properties of TPU (MW ≈ 72 kDa) before and after healing, and optical images of TPU (MW ≈ 32 kDa) healing process.[76] Reproduced with permission from ref. 76, Copyright 2020, Springer Nature.

memory components, *etc.* is relatively straightforward in terms of operation. Nevertheless, a series of pivotal issues that accompany this approach demand due attention. These encompass the interfacial bonding strength between the self-healing elements and the matrix, chemical stability, the efficacy and frequency of healing and so on. Specifically, for super-hard and hard materials, a significant disparity in hardness exists between the self-healing elements (*e.g.*, embedded microcapsules) and the matrix, exacerbated by a weak interfacial bonding strength. Under external loading, the interface of such materials is highly susceptible to stress concentration, which in turn leads to the initiation interface cracking. Therefore, a trade-off between material properties and self-healing properties is needed to meet the demands of the working conditions.

2.2 Intrinsic self-healing mechanisms

Intrinsic self-healing relies on its own internal structure or physicochemical properties to achieve self-healing. In contrast to extrinsic self-healing, intrinsic self-healing usually repairs scratches or undetectable defects at the crack nucleation stage and can theoretically be repeated over and over again. In the case of superhard materials, due to their intrinsic brittleness, fracture failure occurs in the event of microcracking. Therefore, studying the intrinsic self-healing mechanism is highly significant for addressing the safety and reliability of superhard materials and their related applications. So far, some progress has been made in the study of intrinsic healing mechanisms, such as dynamic covalent bonding, supramolecular interactions, defect-driven self-healing, phase transitions, and so on.

2.2.1 Dynamic covalent bonds. Permanent covalent bonds are relatively stable and require substantial energy to break. Once broken, they are challenging to re-bond under relatively mild conditions. In contrast, dynamic covalent bonds can be reversible bonded under certain temperature, PH, light and other effects after breaking, demonstrating their dynamic nature.[77–79] The process of dynamic bond exchange can be divided into two types, namely "dissociative" process and "associative" process.[80] The Diels–Alder (DA) reaction is one of the most well-known reversible covalent bond reactions, specifically referring to the [4+2] cycloaddition reaction between a dienophile and a prodienophile. Firstly, at a sufficiently high temperature, the covalent bond breaks, resulting in an inverse reaction known as the retro-DA reaction; subsequently, when cooled to a lower temperature, the cyclisation reaction occurs again (DA reaction) and the covalent bond re-forms, eventually healing itself. In 2002, Wudl *et al.* developed a self-healing polymer material based on thermally reversible DA reaction, which was prepared by DA cycloaddition of thermally reversible dienes (polyfuran, F) and polydienes (polymaleimide, M).[81] The DA reaction of furan and maleimide can form a highly cross-linked network. At temperatures above

120 °C, about 30% of the "inter-unit" connections break, but reconnect and self-heal upon cooling. Faseela *et al.* imparted self-healing properties to the composites by designing maleic anhydride-grafted polystyrene-*block*-poly (ethylene-ran-butene)-*block* polystyrene, enabling the formation of strong reversible covalent bonding (DA reaction) with furfuryl alcohol.[82] Wang *et al.* designed a repairable and separable carbon nanotube (CNT)/graphene oxide (GO)/polyurethane (PU) composite (CG@CPA) using an electrostatic assembly strategy, which is cationic aqueous polyurethane (CPA) with Diels–Alder bonds.[83] The CG@CPA composite with microcracks (~83 μm) were heat-treated (130 °C) to temporarily split into low molecular weight material through the retro-DA reaction ("dissociative" process), which re-bonded the fractured portions; subsequently, they were kept at 60 °C for 2 h to re-cross-link the cracked molecular chains through the DA reaction ("associative" process), and the fractured conductive network was reconstructed to achieve self-healing (Fig. 5a and b). After three cycles of healing, the electrical conductivity decreased by only 10% and the healing efficiency of the mechanical properties was still 95% (Fig. 5c and d).

In addition to DA reactions, dynamic covalent bonds used for the development of self-healing materials include disulfide bonds, boron ester bonds, imine bonds, *etc.*[86–89] Disulfide bonds can be rapidly exchanged between disulfide or between disulfide and thiols, whose dynamic covalent properties can be stimulated by a variety of external stimuli such as sound, light, thermal and mechanical energy.[90–92] Self-healing materials such as soft gels, elastomers, *et al.* with self-healing properties can be obtained by embedding disulfide bonds in polymer materials.[93,94] For example, Lai *et al.* developed self-healing polyurethane elastomers with disulfide bonds (PUDS) by embedding and locking dynamic disulfide bonds in viscoelastic hard microphase regions, which healed surface scratches within 60 s at 70 °C, and achieved a healing efficiency of 85% at 70 °C for 6 h after complete fracture (Fig. 5e–g).[84] Dynamic covalent bonding boron ester bonds can be obtained by hydrolysis reactions, ester exchange reactions with exogenous substances and exchange reactions between different boron ester compounds.[88,95,96] The B–O bonds can be exchanged through both thermo-activated direct metathesis between different boronic ester compounds and water-assisted hydrolysis/dehydration. For example, Ma *et al.* endowed a cholesteric liquid crystal elastomer (CLCE) with programmable and self-healing capabilities by introducing boron ester bonds into CLCE polymer networks, which was attributed to the reversible B–O bond exchange carried out by water-assisted hydrolysis/dehydration

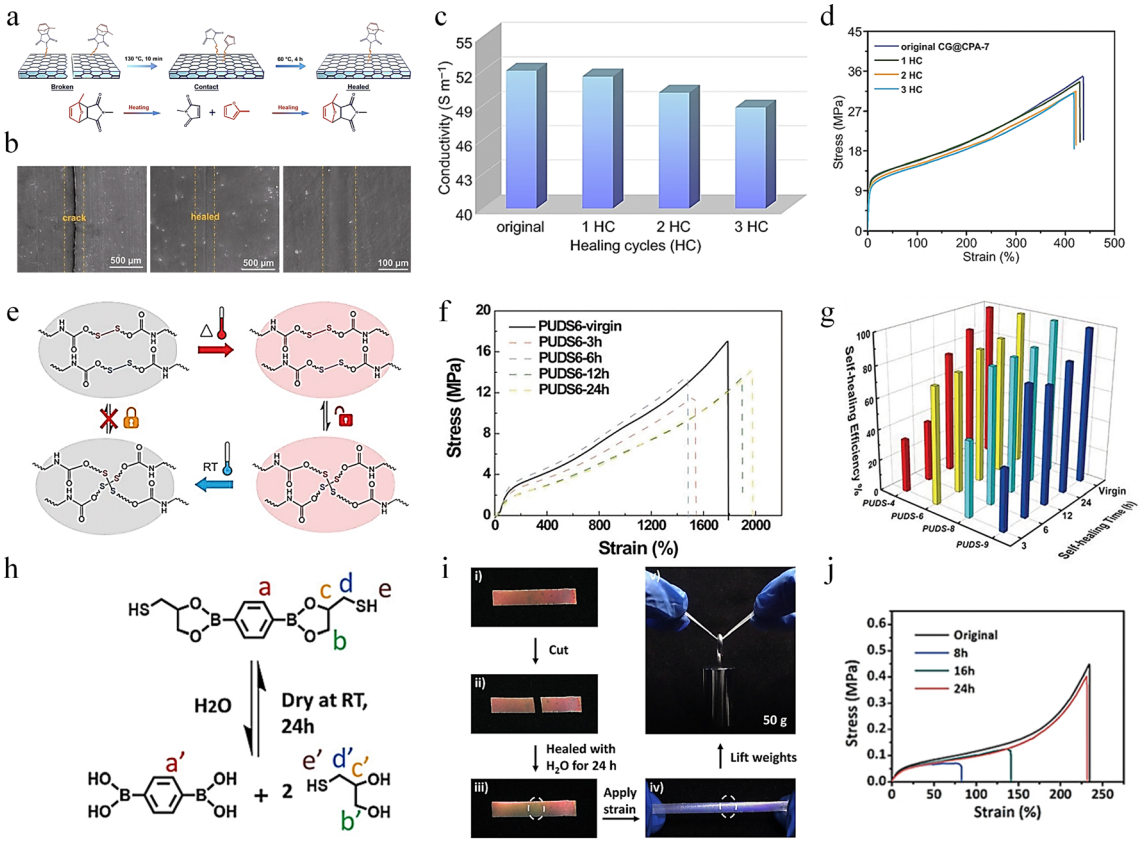

Fig. 5 Research on self-healing materials based on dynamic covalent bonds. (a)–(d) The mechanism, healing process and self-healing tests of CG@CPA.[83] Reproduced with permission from ref. 83, Copyright 2021, Springer Nature. (e)–(g) Self-healing mechanism diagram and self-healing tests of PUDS bulk material samples.[84] Reproduced with permission from ref. 84, Copyright 2018, Wiley-VCH. (h)–(j) Schematic mechanism, optical image of the self-healing process of fractured CLCE and stress–strain curve with different healing time.[85] Reproduced with permission from ref. 85, Copyright 2022, Wiley-VCH.

(Fig. 5h).[85] The fractures of completely broken CLCEs were joined together and a few drops of water were added to the damaged interface, followed by close contact at room temperature for 24 h (Fig. 5i). The samples self-healed with a maximum healing efficiency of 86.18% (Fig. 5j). The imine bond is capable of three dynamic transformations: transamination, decomposition of imine complexes, and hydrolysis, which can endow materials with the properties of self-healing, solderability, and degradability.[97–99] Bhattacharya *et al.* endowed the gel with self-healing properties by generating imine bonds through Schiff base reactions between aldehyde units on the surface of the carbon dots and primary amine residues in the polyethyleneimine network.[100] The addition of water or heating can both enhance the self-healing process.

2.2.2 Supramolecular interactions. Compared to dynamic covalent bonding, non-covalent supramolecular interactions have lower ''dissociative'' and ''associative'' energies, and therefore require milder conditions for re-bonding upon rupture, and enabling self-healing at room temperature without external stimuli. Non-covalent supramolecular interactions, including hydrogen bonding, π–π stacking, and host–guest interactions, can also contribute to the self-healing process. These weak interactions can readily reform upon damage, facilitating the recovery of material properties. In the development of self-healing materials, the reversibility, directivity and sensitivity of supramolecular interactions make them attractive. For example, self-healing designs that utilize hydrogen bonds can leverage the excellent mechanical strength derived from their directivity and high unit volume concentration, along with their reversibility, to achieve self-healing of thermoplastic polymers.[101–103] Gao *et al.* combined decuple hydrogen bonds with soft polydimethylsiloxane (PDMS) chains to prepare a carbonyl hydrazone (CHZ)-based strong dynamic decuple hydrogen bond. After healing for 24 hours at 70 °C, the healing efficiency reached approximately 100%, demonstrating excellent self-healing capability in CHZ-PDMS.[104] Zhang *et al.* improved the high self-healing ability of hybrid conductive hydrogels through multiple hydrogen bond interactions.[105] Furthermore, quadruple hydrogen bonding can provide a higher association constant, thus enhancing the strength of association between units.[106,107] For example, Chen *et al.* investigated the effects of dynamic disulfide bond metathesis (HEDS) and supramolecular cross-linked tetrahydrogen bond (UPy) on the properties of dynamic supramolecular elastomers (DSE).[108] With the increase of healing time at room temperature, the final self-healing stress can reach nearly 92.76%, and the strain after 48 h basically overlaps with that of the original sample (Fig. 6a). Increasing the temperature speeds up the self-healing process, which is due to the dynamic disulfide bond exchange reaction and the recombination of multiple H-bonding interactions in the polymer chain are more likely to occur at higher temperatures (Fig. 6b).

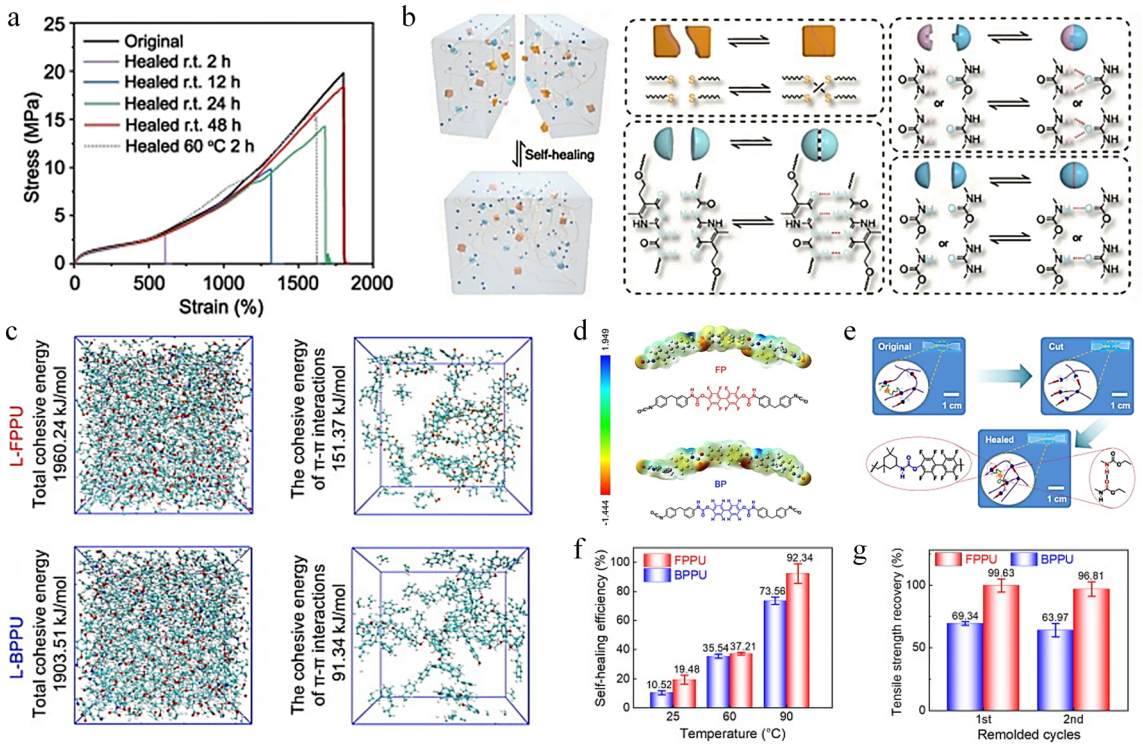

Fig. 6 Research on self-healing behavior based on H-bonding and π–π stacking interaction. (a) and (b) Test of mechanical properties of DSE before and after healing, and schematic diagram of healing mechanism.[108] Reproduced with permission from ref. 108, Copyright 2022, Springer Nature. (c) and (d) Molecular dynamics simulation and electrostatic potential calculation of L-FPPU and L-BPPU systems. (e) Schematic diagram of FPPU and BPPU healing mechanism. (f) and (g) Self-healing efficiency and recovery efficiency of tensile strength for FPPU and BPPU.[109] Reproduced with permission from ref. 109, Copyright 2024, Elsevier.

π–π stacking is a weak intermolecular interaction exhibited by π-electron conjugated systems under certain specific spatial arrangements. This type of interaction plays a significant role in molecular structure, reaction mechanisms, and optical properties. In aromatic compounds, π–π stacking is a special spatial arrangement that typically occurs between two molecules that are relatively electron-rich and electron-deficient, making it an important non-covalent interaction akin to hydrogen bonding. The interaction between the aromatic rings, the π–π stacking, helps to strengthen the non-covalent interaction of the polymer chains.[110] According to Jia *et al.*, fluorine atoms exhibit a stronger electron-pulling induction effect than hydrogen, and connecting fluorine atoms directly to the aromatic ring changes the π–π stacking pattern and enhances the π–π stacking interaction.[109] They produced a fluorinated phenolic polyurethane (FPPU) elastomer based on octafluoro-4,4′-biphenol. The internal energy and electrostatic potential of linear fluorinated phenolic polyurethane (L-FPPU) and its non-fluorinated linear bisphenol phenolic polyurethane (L-BPPU) were compared by molecular dynamics (MD) simulations and electrostatic potential calculations (Fig. 6c and d), demonstrating that fluorine atoms further enhance the π–π stacking interaction of aromatic rings. The chopped FPPU material exhibits complete self-healing behavior when subjected to temperature and pressure. (Fig. 6e). FPPU has higher self-healing efficiency than BPPU (92.3% for FPPU and 73.56% for BPPU in Fig. 6f) and tensile strength recovery efficiency (96% for FPPU and 63% for BPPU in Fig. 6g).

Complex interfacial supramolecular interactions will occur at the interface of two different phases (such as solid and liquid or gas and liquid), including hydrogen bonding, π–π stacking, van der Waals forces, electrostatic interactions, hydrophobic interactions, and host–guest interactions. The characteristics of interfacial supramolecular interactions include high selectivity, reversibility and dynamics, which play a key role in regulating interfacial properties such as wettability, adhesion and mechanical properties.[111–114] Xu *et al.* designed a non-covalent assembly of rigid 2D transition metal carbide/carbonitride (MXene) nanosheets based on the layered structure of biological tissues, and prepared a polyurea-carbamate (SHPU)/L-MXene composite (SHPULM).[115] The mechanical properties of SHPULM composites are significantly improved due to the advantages of layered structure and dense interfacial supramolecular interactions. SHPULM is capable of self-healing autonomously and efficiently at room temperature and can be stretched to 5 times its original length after 5 minutes of healing (Fig. 7a). The fractured MXene

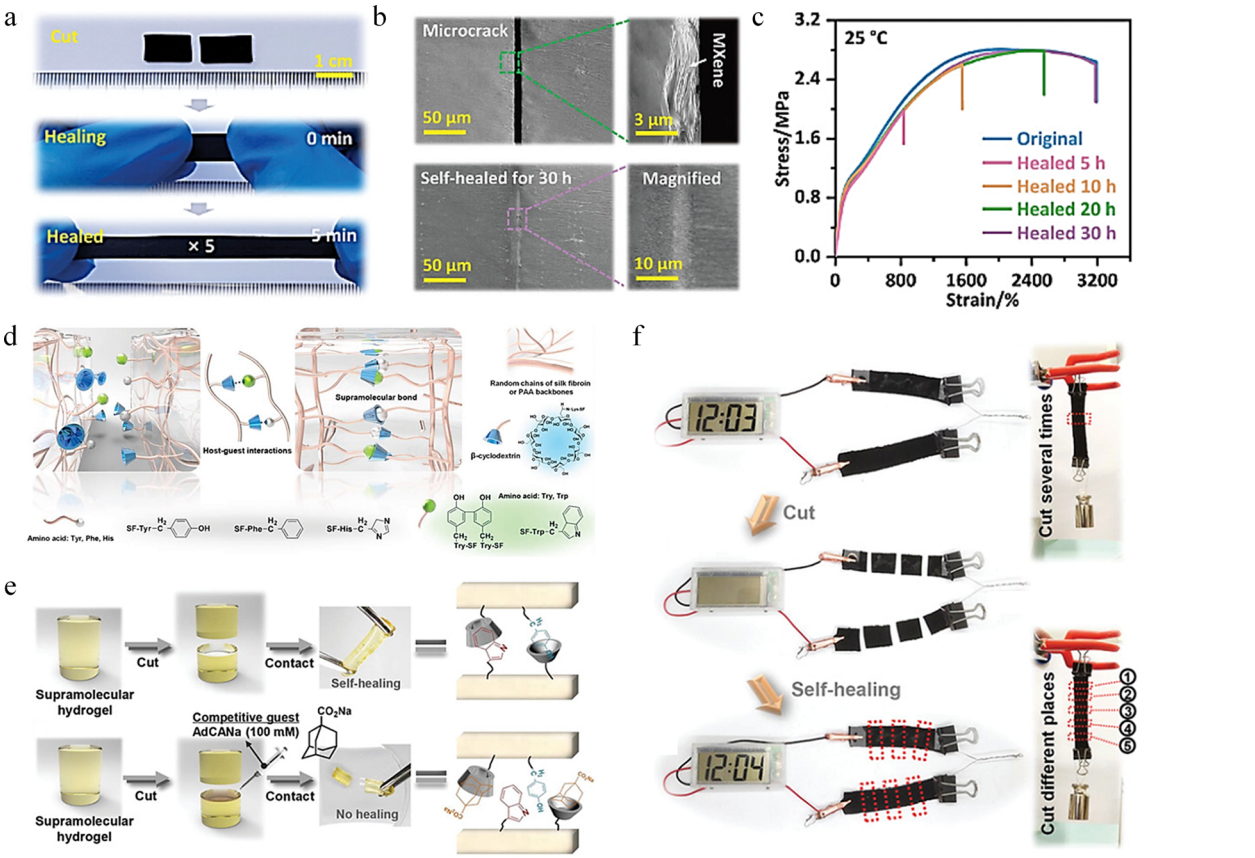

Fig. 7 Research on self-healing behavior based on interfacial supramolecular interaction and host–guest interaction. (a) Photos of SHPULM-20 in instantaneous self-healing and stretching. (b) SEM images of cracks of SHPULM-20 composites before and after self-healing at 25 °C for 30 hours. (c) Stress–strain curves of original and healed SHPULM-20 under different healing time.[115] Reproduced with permission from ref. 115, Copyright 2023, Wiley-VCH. (d) Self-healing mechanism of the supramolecular hydrogels. (e) Self-healing photos of supramolecular hydrogel in a wet and a competitive guest condition. (f) Self-healing behavior of the integrated supramolecular supercapacitor.[119] Reproduced with permission from ref. 119, Copyright 2021, Wiley-VCH.

skeleton can fully heal on a microscale after 30 hours of self-healing at 25 °C, as shown in Fig. 7b. The stress–strain curve in Fig. 7c indicates that the recombined SHPULM repaired at room temperature for 30 h almost overlapped with the original curve with self-healing efficiency of 97 ± 2%. In supramolecular chemistry, host and guest molecules interact through non-covalent bonds to form stable complexes. The strength and nature of the host–guest interaction can be modulated by changing the chemical structure of the subject or the guest, which provides a wide range of tunability for the design of materials.[116–118] The Mo *et al.* fabricated a supramolecular hydrogel with host–guest complexes of two types of β-cyclodextrin (β-CD) using an entirely elastic and entirely polymeric approach, which possesses excellent self-healing characteristics.[119] Fig. 7d illustrates the self-healing mechanism of the supramolecular hydrogel: the residual amino acid molecules on the surface of the supramolecular hydrogel sheets interact with the grafted β-CD molecules, forming supramolecular bonds within the double-cross-linked hydrogel through host–guest interactions. Fig. 7e demonstrates that when cut hydrogel blocks are brought into contact under humid conditions, allowing the blocks to fully heal within 1 hour. In contrast, healing does not occur in a competitive guest solution because the competitive molecules occupy the β-CD, thereby inhibiting its self-repair characteristics. This demonstrates the intelligent response of supramolecular hydrogels to different environmental stimuli. Then, they tested the self-healing behavior of the supramolecular hydrogel integrated capacitor (Fig. 7f). After being cut and standing for 1 hour at ambient condition, it could still power an electronic watch. Even after being cut 30 times in a cycle, it could still support a weight of 500 g without breaking and maintain 95.8% of its capacitance, indicating that the supramolecular hydrogel capacitor has excellent self-healing characteristics.

2.2.3 Diffusion behavior. Diffusive behavior is necessary for most self-healing materials and increasing the rate of diffusion helps to drive the self-healing process. In polymers, interchain diffusion behavior is crucial to their self-healing process, primarily because this process relies on the interfacial molecular diffusion of polymer chains to fuse cracks.[120] By decreasing the molecular weight of the linear polymer or the crosslink density of the network, the mobility of the chains can be increased, which in turn accelerates the healing process.[121] Molecular mobility and effective diffusion across the polymer interface are key requirements for healing of metallosupramolecular polymers.[122] Even, based on the intrinsic properties of polymers, self-healing using interchain diffusion mechanisms.[123–125] In addition to polymers, diffusion mechanisms feature prominently in the self-healing behavior of perovskite materials.[126] Loosely bonded halide ions in the perovskite material migrate around the major ion lattice and interact with the electric field during cell operation, leading to the creation and migration of gap and vacancy defects. High-energy defects and structural losses cause crystal decomposition, reversible structural self-healing occurs in the dark state, and redistribution of migrated ions and recovery of photocurrent occur during the initial degradation self-healing process.[127,128] Perovskite have high ion mobility and low crystal formation energy at grain boundaries and lattices, which are more conducive to self-healing than other inorganic semiconductors.[129,130] For monocrystal ionic bonding materials, such as methylammonium lead(II) iodide ($MAPbI_3$). Al-Handawi *et al.* split a large single crystal sample of $MAPbI_3$ into two halves using a razor blade, cutting perpendicular to the (100) crystal plane and parallel to the (001) crystal plane. The sample was then maintained in a nitrogen atmosphere for 24 hours while a series of minimum stresses (0.65–1.5 N) were applied to ensure contact. The lattice behaves like a liquid due to the soft structure of the $MAPbI_3$ ionic component. After fracture, the stress-induced ions have high mobility at the interface at room temperature, thus achieving morphological recombinationas, and the simulation schematic is shown in Fig. 8a. The final mechanical property healing efficiency reaches 82% and the generated photocurrent recovery rate reaches 74% compared to the initial state.[131] The addition of polymers has practical implications for ameliorating macroscopic mechanical failures in perovskite, as the intrinsic properties of polymers balance strong intermolecular forces with high chain mobility to give the material flexibility and self-healing capabilities. In the damaged polycrystalline chalcogenide polymer composite film material $MAPbI_3$, a significant increase in the ion diffusion rate was induced by the application of compressive stress and appropriate thermal activation, leading to the repair of the broken interface.[132]

Finkenauer *et al.* doped thiourea-triglycol polymer molecules with mechanical toughness and self-healing into polycrystalline chalcogenide films, and synthesised chalcogenide films with glass transition temperatures close to room temperature and strong interactions with chalcogenide to form composites with bicontinuous interpenetrating networks. The TUEG3 polymer in the active layer was found to contribute to the reattachment of distant chalcogenide particles and repair of large cracks. This is due to the softening effect of the polymer addition, which promotes the mechanisms of synergistic grain growth and solid diffusion to repair the damage, as shown in Fig. 8b. The healing ability of the films exhibited differences with the addition of different contents of polymer molecules.[133] Structural healing processes due to diffusion phenomena have also been of wide interest in the field of metallic materials, most of which are categorised as cold welding. Cold welding is a process of welding metals at near ambient temperatures (usually under atmospheric pressure) that requires clean and flat metal surfaces to be contacted under vacuum conditions to produce atomic diffusion leading to strong adhesion. Additional conditions generally need to be imposed, such as mechanical vibration, pressure, electrical impulses to induce the breakdown of the original stable atomic bonds on the metal surface. Consequently, atomic diffusion occurs at the separated interfaces on both sides, resulting in the formation of new bonds and leading to structural healing. Some experiments have been conducted by applying pressure to copper wires to eventually achieve the fusion of their ends at the point of contact.[135] Nanomaterials such as nanoparticles, metal films or nanowires, have been found to exhibit cold welding behaviour. Rapid atomic rearrangements, surface diffusion, and atomic hopping are the fundamental

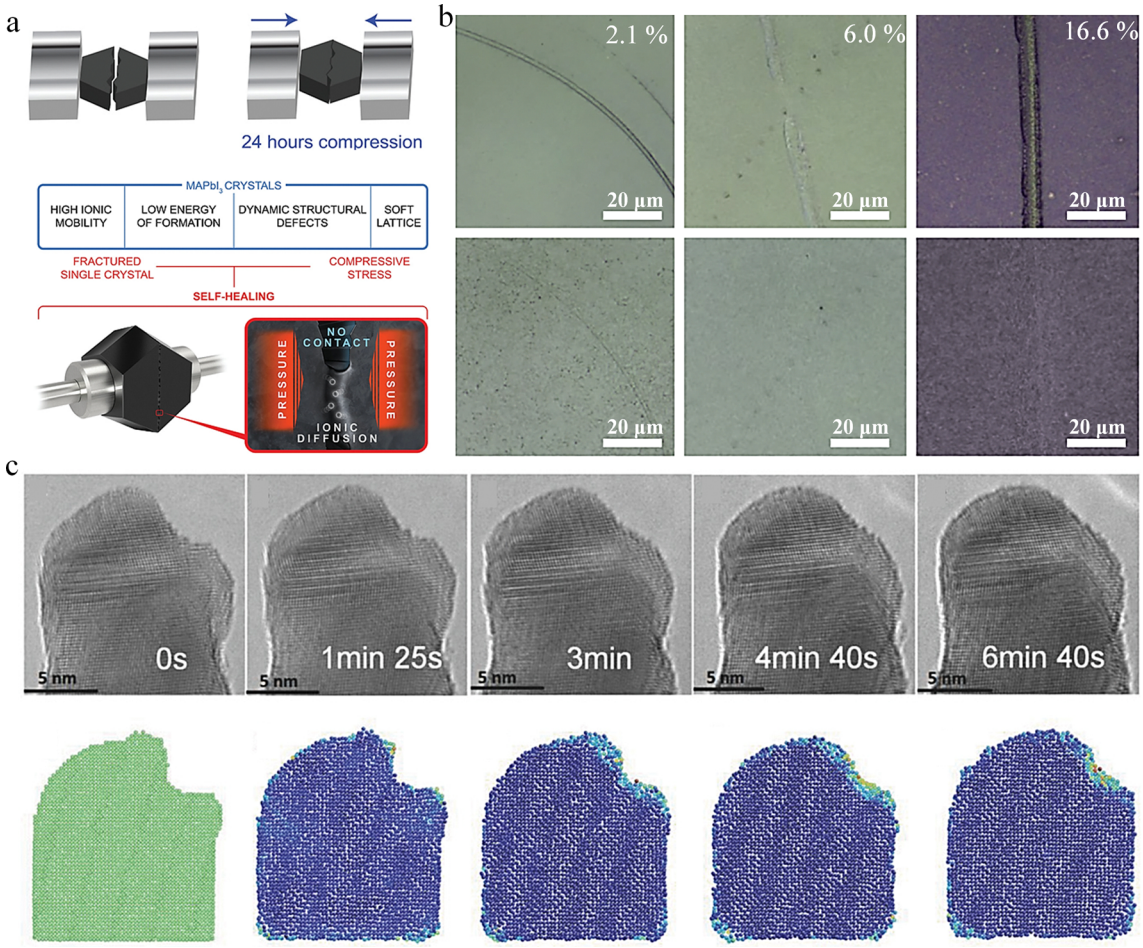

Fig. 8 Structural self-healing behavior due to diffusion occurring in different types of materials. (a) Schematic representation of the method used for self-healing and mechanism of self-healing of $MAPbI_3$.[131] Reproduced with permission from ref. 131, Copyright 2022, Wiley-VCH. (b) Optical image of material surface damage when untreated and after heating at 100 °C for 1 h using different polymer mass percentage.[133] Reproduced with permission from ref. 133, Copyright 2021, Elsevier. (c) Surface diffusion behaviour of gold nanowire.[134] Reproduced with permission from ref. 134, Copyright 2018, Wiley-VCH.

modes for atomic transport on nanoscale metal surfaces.[136] Wang *et al.* found that the cold welding process of gold nanowires can be assisted by simple mechanical vibration, and Fig. 8c shows that after using a tungsten probe to leave a crater at the fracture of a gold nanowire, the surface geometry of the end surface of the nanowire was reconstructed by a surface atomic diffusion process, which ultimately exhibits the pre-damage morphology. The surface atomic diffusion process can be accelerated with the addition of mechanical vibration assistance to achieve fusion of the nanowire fracture ends.[134]

2.2.4 Defect-driven processes. Defects in the crystal structure, such as vacancies and dislocations, can act as active sites for self-healing. Diffusion and recombination of atoms at these defects can lead to the restoration of the material's integrity, especially in metallic materials. In metallic materials, the internal microstructure evolves during service until failure occurs. Two primary strategies exist to enhance the self-healing performance of these materials: (1) autonomous self-healing of nanoscale defects to prevent catastrophic failure, and (2) repair of internal damage through external field stimuli, such as heat, magnetic fields, and pressure.[58,124] Autonomous self-healing of materials is accomplished by precipitation at high temperatures, *e.g.* in steel[137] and aluminum-based materials such as aluminium alloys.[138] Defective cavities act as the initial location of material damage during creep, especially at grain boundaries. The composition is designed so that oversaturated solute atoms fill the nano-defects by dislocation transfer, and the precipitation phase nucleates around the defective cavities, which not only prevents the further growth of the defective cavities but also fills them internally, ultimately enabling the complete filling of the cavities and the self-healing of the material. Assisted self-healing involves introducing external field conditions, such as raising the temperature below the melting point. This phenomenon has been observed in single crystal gold[139] and porous silver[140] under elevated-temperature annealing conditions, leading to complete recovery of plastic deformation in the material. In the pure iron crack healing process, increasing the temperature enhances the atomic mobility and improves the healing efficiency. It has further been shown that in mild steel, additional compressive stresses applied at 900 °C below the recrystallisation and grain growth temperatures

generated raised particles on the crack surface, leading to crack cutting, size reduction and eventual healing of the pores by gradual filling.[141] Another strategy is to introduce an electric field environment that increases the atomic mobility at the defect location and promotes internal crack repair. Zang *et al.* combined nanoindentation with an atomic force microscope (AFM) system equipped with a diamond indenter to monitor the electrical self-healing behaviour of mechanically damaged ZnO nanoribbons with *in situ* electrical measurements. As shown in Fig. 9a, the AFM images of the plastically deformed ZnO nanoribbons are shown, and the high-resolution transmission electron microscopy (TEM) images indicate that cracks and a large number of dislocations have been generated within ZnO. Further mechanism maps explain the formation of high-density dislocations in the violently deformed zone caused by the indenter. In the Fermi energy level pinning model, assuming that a row of deep energy levels depleting the free charge in ZnO is distributed radially from the dislocations to the depletion boundary, the high-density dislocations correspond to the depletion regions were heavily overlapped in the energy band diagrams, which resulted in a significant decrease in the electrical conductivity and the non-linear *I–V* behaviour. As the dislocations moved out of the material during the healing process, the density of dislocations and the regions affected by plastic strain decreased significantly and the depletion regions were no longer overlapped, resulting in an electronic structure that was only partially affected by the potential barrier. The whole process utilises electrical pulses to generate local current heat at the defect location, helping the defect and the atoms to overcome the energy barrier to diffusion, and applying localised thermocompressive stresses over a temperature gradient to repair the crack damage.[142] Oleg Kovalenko *et al.* used nanoindentation to cause plastic deformation damage in gold microparticles, the deformation damage was almost completely repaired after high-temperature annealing treatment, and the results of molecular dynamics simulations, shown in Fig. 9b, revealed that the atomic diffusion to be predominately

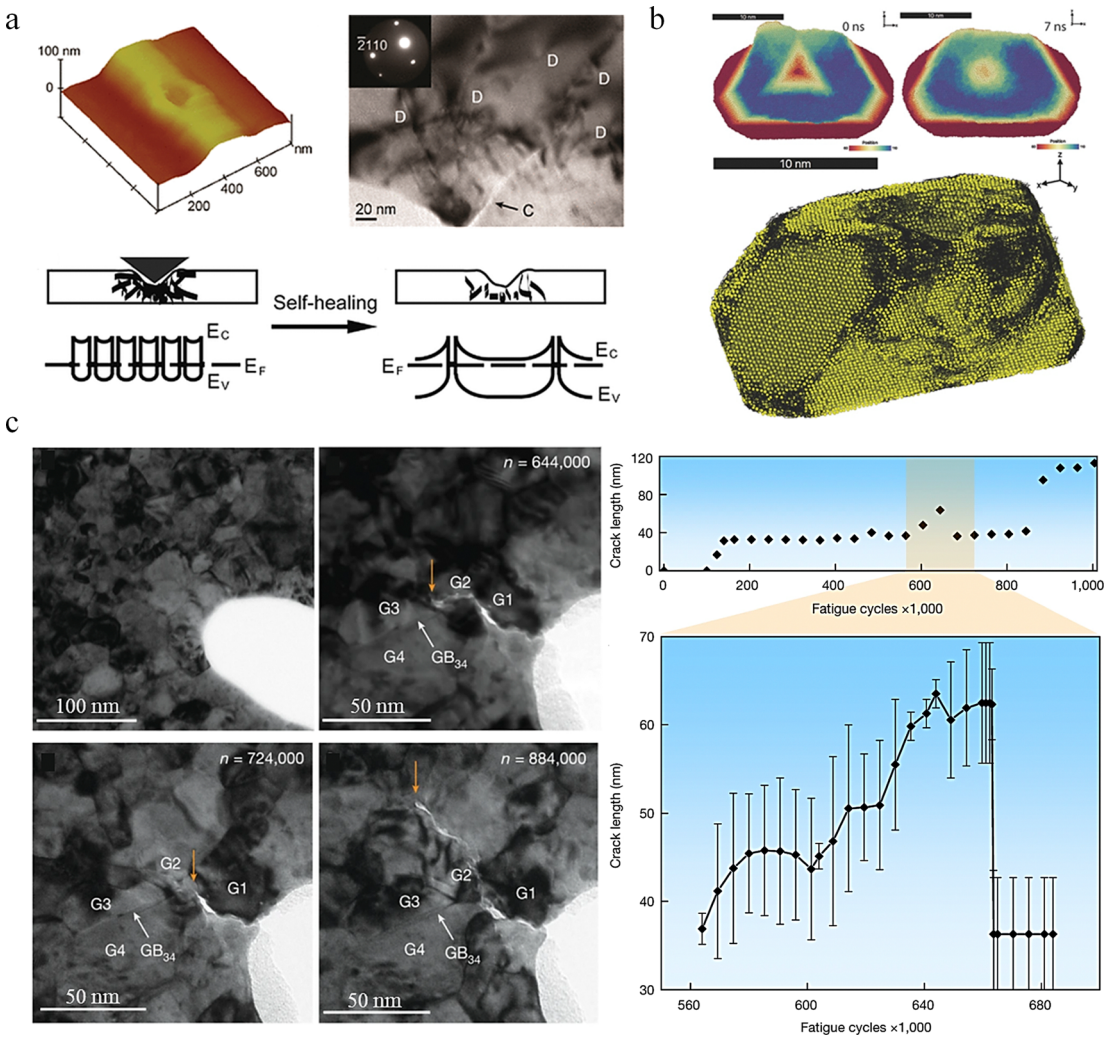

Fig. 9 Mechanisms of structural internal defects and microstructural effects on the self-healing behaviour of metals. (a) The self-healing behavior of ZnO nanobelt. D: dislocations, C: crack.[142] Reproduced with permission from ref. 142, Copyright 2011, American Chemical Society. (b) Damage recovery from plastic deformation of gold particles.[139] Reproduced with permission from ref. 139, Copyright 2017, Wiley-VCH. (c) Self-healing behaviour of polycrystalline Pt.[143] Reproduced with permission from ref. 143, Copyright 2023, Springer Nature.

along the slip traces, the geometric edges between the facets, and on the minority.[139] Recent studies have demonstrated that self-healing under unaided external field conditions can depend on defects in the grain boundary microstructure of the material. Self-healing of nanoscale fatigue cracks occurs in nanocrystalline Pt, Christopher M. Barr *et al.* found crack flank cold welding induced by a combination of local stress state and grain boundary migration. Crack healing occurred by closure and cold welding of the crack faces under the influence of internal stresses generated by localized grain boundary migration. Fig. 9c shows that during crack initiation and extension during fatigue stretching, crack healing occurs at the triple junctions of the grains, resulting in significant crack deflection. Crack healing presumably occurs at cycle 664 000 of cyclic loading. The presence of small-size twin boundaries is close to the crack healing region (GB34). Statistical graph shows the variation of crack length with emergence, extension, and self-healing behaviour during the complete cyclic loading process.[143]

In contrast to the extrinsic self-healing mechanism, the intrinsic self-healing mechanism operates on a distinct principle. It primarily relies on dynamic covalent bonds, supramolecular interactions, and atomic diffusion processes to exert its effectiveness. The relatively low bond energies involved in these processes allow the material to spontaneously undergo the cleavage and recombination of chemical bonds or the re-establishment of atomic/molecular interactions, either in the absence of external stimuli or with minimal energy input. Notably, the intrinsic self-healing mechanism effectively overcomes the limitation of the restricted number of healing cycles in the extrinsic mechanism. Moreover, it circumvents a series of issues arising from the interface mismatch between self-healing elements and the matrix. Consequently, by capitalizing on the advancements in the intrinsic self-healing mechanisms, the precise modulation of bond energies in super-hard covalent materials to align with the activation conditions of this mechanism— or the incorporation of chemical bonds capable of facilitating the autonomous re-bonding of fractured bonds—could play a pivotal role in the design of superhard covalent materials with self-healing properties.

3. Research on novel self-healing superhard covalent bond materials

3.1 Development of novel superhard materials

Hardness refers to the combined resistance of the chemical bonds in a crystal to indentation.[46] The superhard properties derive from their unique microstructure and ultra-strong permanent covalent bonds. Following the successful development of polycrystalline diamond (110–140 GPa) (Fig. 10a), which exceeds the hardness of monocrystalline diamond,[144] Tian *et al.* prepared nanotwinned diamond (200 GPa) (Fig. 10b) with

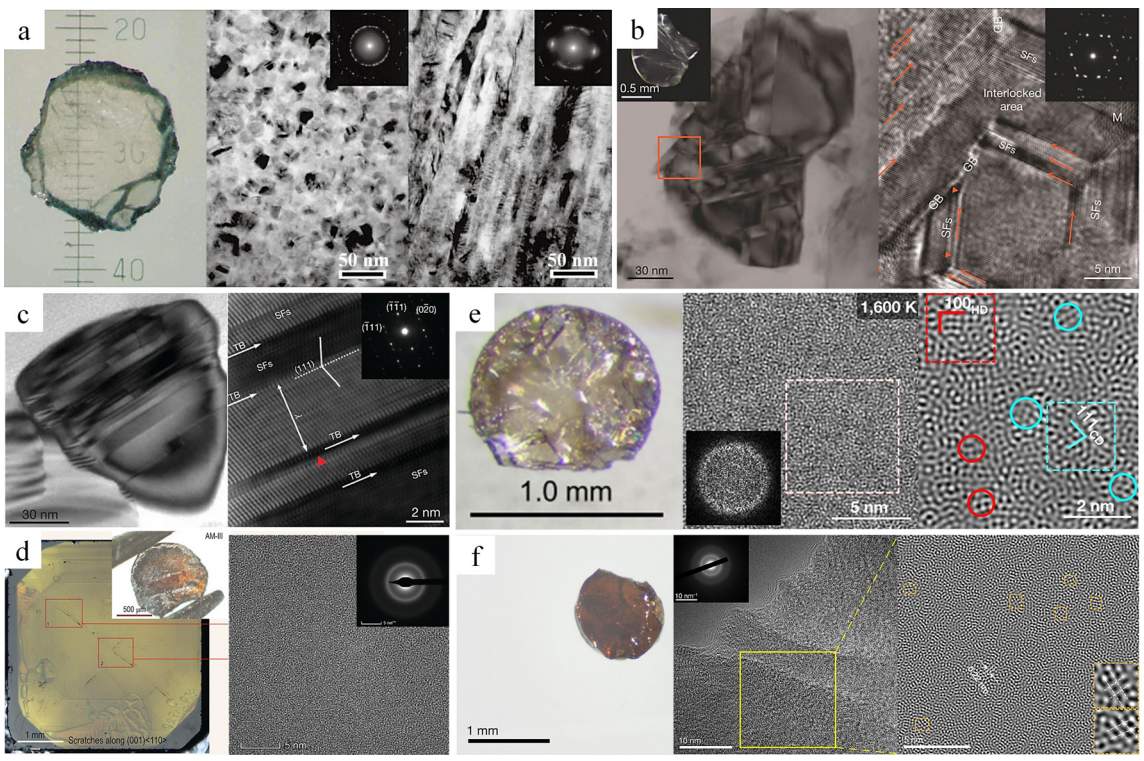

Fig. 10 Superhard materials. (a) Polycrystalline diamond.[144] Reproduced with permission from ref. 144, Copyright 2003, Springer Nature. (b) Nanotwinned diamond.[145] Reproduced with permission from ref. 145, Copyright 2014, Springer Nature. (c) Nanotwinned cubic boron nitride.[50] Reproduced with permission from ref. 138, Copyright 2013, Springer Nature. (d) AM-III.[146] Reproduced with permission from ref. 146, Copyright 2021, Oxford University Press. (e) Paracrystalline diamond.[147] Reproduced with permission from ref. 147, Copyright 2021, Springer Nature. (f) AC-3.[148] Reproduced with permission from ref. 148, Copyright 2021, Springer Nature.

hardness up to twice that of natural diamond, and nanotwinned cubic boron nitride (Fig. 10c) with hardness exceeding 100 GPa through the introduction of nanotwinned microstructural design.[50,145] These superhard materials have a three-dimensional bond network with short and strong bonds, high bond density and high valence electron density.[47] Subsequently, amorphous carbon materials (AM-III) (Fig. 10d) with a high content of sp^3 hybridization (~94%) that can scratch single crystal diamond were developed.[146] In addition, polycrystalline diamond (Fig. 10e) and amorphous carbon (AC-3) (Fig. 10f), which also have a high proportion of sp^3 hybridized carbon, have been reported.[147,148] Without exception, these superhard materials are composed of ultra-strong permanent covalent bonds. However, a significant issue that is increasingly apparent is the intrinsic brittleness of the material, where even a small crack can lead to catastrophic fracture damage, resulting in structural material deterioration and posing serious risks to the safety and reliability of superhard materials and their associated devices. Yue *et al.* successfully prepared nanotwinned diamond composites (ntDC) assembled with coherently interfaced diamond polytypes, interwoven nanotwins and interlocked nanograins, and increased the fracture toughness to 26.6 MPa $m^{1/2}$ without sacrificing hardness (~200 GPa), which is five times higher than that of synthetic diamond.[149]

To expand the application fields of superhard materials, researchers have been constantly searching for superhard materials other than diamond and cubic boron nitride. Recently, Tian *et al.* carried out research on grain refinement of cubic silicon carbide (SiC). They found that when the grain size of this material was refined to 10 nanometers, its hardness reached 41.5 GPa.[51] This discovery implies that this category of silicon carbide meets the hardness criteria for superhard materials and can be classified as such. In fact, apart from silicon carbide, the hardness of certain diamond-like films, carbon nitrides, and other materials can also reach 40 GPa or even higher.[150,151] In recent years, researchers have carried out predictions and explorations of potential superhard materials by means of theoretical calculations and other methods.[152,153]

In the research of superhard materials, researchers mainly focus on two key aspects. Firstly, through nanostructure design, such as nanotwins and gradient interfaces, the internal structure is optimized to increase hardness and improve toughness.[52,154] Secondly, theoretical models of hardness are developed, alongside the exploration of new superhard phases, to push the boundaries of traditional materials and overcome their inherent limitations.[47,155] Despite remarkable achievements, the proportion of superhard materials in practical applications is low. The inherent brittleness of high hardness materials makes them highly susceptible to the initiation and propagation of microcracks during long-term service due to external factors such as wear or impact. This, in turn, shortens the service life of the materials and makes it difficult to ensure their reliability. Meanwhile, the complexity of atomic bonding and phase-transformation kinetics hinders the optimization of the hardness of existing materials, and the synthesis of materials predicted by theory is also restricted by technical issues such as thermodynamic instability. Therefore, the coordinated regulation of hardness, toughness, and stability within the existing material system has become a central challenge in the field. The bionic self-healing mechanism, which draws on the self-healing characteristics of organisms, is expected to endow materials with self-healing capabilities and provide new ideas for solving the above-mentioned problems.

3.2 Study of self-healing superhard covalent bonding materials

In the previous chapter, we conducted a systematic and in-depth exploration of the existing self-healing mechanisms, covering both extrinsic and intrinsic self-healing mechanisms. These research findings provide ideas for the development of novel self-healing superhard covalent bond materials. However, numerous formidable challenges lie ahead. Common synthesis methods for superhard materials, such as high temperature and high pressure methods, chemical vapor deposition, *etc.*,[44] encounter significant difficulties when incorporating self-healing elements (*e.g.*, microcapsules and shape memory alloys). Under high temperature and high pressure synthesis conditions, the microcapsule wall materials may fail to withstand the extreme environment, resulting in the inability to effectively encapsulate the healing agents. Moreover, achieving uniform dispersion of microcapsules within the matrix remains a highly challenging task. When microcapsules are introduced using chemical vapor deposition, the surface quality of the coating may be compromised, leading to surface irregularities or defects. Additionally, due to the weak interfacial bonding force between the microcapsules and the coating, detachment is prone to occur. If shape memory alloys are incorporated into superhard materials, due to the obvious mismatch in coefficient of thermal expansion among these constituent phases,[156,157] significant thermally-induced mismatch stress is likely to arise at the heterogeneous interface. This stress concentration effect tends to trigger interfacial delamination or microcracks, thus severely undermining the structural integrity and thermomechanical stability of the composite materials.

Oxidation healing mechanisms rely on high temperatures and an air/oxygen environment, which is unfavorable for diamond. This is due to the poor thermal stability of diamond. Graphitization of diamond begins when the temperature exceeds approximately 780 °C.[158] Moreover, neither diamond nor cubic boron nitride can form oxides to heal cracks. However, this oxidation healing mechanism appears to be applicable to SiC. When SiC undergoes oxidation at high temperatures (~800 °C), it transforms into SiO_2, which can fill the cracks in the material. Nevertheless, there is a substantial difference in hardness between the hardness of SiO_2 (10.9 GPa) and that of pure SiC (33.3 GPa).[159,160] More crucially, precisely controlling the high-temperature oxidation healing process exclusively at the sites where microcracks occur in SiC remains a significant challenge.

The defining feature of ultra-hard covalent bonds is their extremely high hardness. This property indicates a higher bond density/electron density, shorter bond lengths, and a greater degree of covalency.[161] For instance, the super-strong C–C covalent bonds in diamond are among the most robust chemical bonds. They allow several carbon atom layers to

withstand pressures up to 40 GPa.[52,162] Unlike metallic materials, it is difficult for these bonds to heal through the atomic diffusion process. Moreover, such permanent covalent bonds have higher dissociation activation energies and binding energies compared to dynamic covalent bonds and supramolecular interactions. Under normal conditions, achieving reversibility is an arduous task. Consequently, the realization of the intrinsic self-healing of superhard covalent bond materials poses a significant challenge. Table 1 summarizes the damage mode, self-healing mechanism, self-healing condition and self-healing efficiency of superhard/hard covalent bond materials. In current research, hard covalent bond materials can achieve self-healing through processes such as oxidative healing, atomic diffusion, re-bonding of permanent covalent bonds, and grain growth. In contrast, given the unique properties of superhard covalent bond materials, we mainly focus on understanding the intrinsic mechanism of the self-healing process induced by the re-bonding of permanent covalent bonds.

3.2.1 Self-healing of diamond. Currently, research on self-healing superhard materials primarily focuses on diamond materials. Yue *et al.* found that when testing the fracture toughness of ntDC by single-edge notched beam (SENB) test, the cracks appeared to heal when the load was unloaded (Fig. 11a).[149] Further, Qiu *et al.* delved into the self-healing behaviour of superhard diamond materials.[163] The fully fractured ntDC nanobeams with width of ~200 nm, without external stimuli, can achieve up to 34% healing efficiency at room temperature simply by putting the fracture in contact (Fig. 11b). The self-healing performance is intricately linked not only to the healing time and frequency of healing but also to the maximum healing efficiency, which is profoundly influenced by the effective contact area when the two fractured surfaces make contact. In ntDC, as cracks initiate and expand, an amorphous carbon region forms at the crack tip. After the material fractures completely, this amorphous carbon distributes on the fracture surface (Fig. 11c). This amorphous carbon structure is composed of a mixture of sp^2 and

Table 1 Summary of recent studies on the self-healing behavior of superhard/hard covalently bonded materials

Superhard/hard covalent bond materials		Damage mode	Self-healing mechanism	Self-healing condition		Self-healing efficiency	Ref.
Nanotwinned diamond composite nanobeam	Width: 200 nm	Completely fractured	Formation of amorphous diamond osteoblasts hybridized by a mixture of sp^2 and sp^3 on the fracture surface, interatomic interaction forces change from repulsion to attraction, C–C re-bonding	Room temperature without pressure, high vacuum	Helaing time: 600 min	34.1%	163
	Width: 300 nm				Helaing time: 60 min	24.2%	
	Width: 400 nm				Helaing time: 60 min	18.4%	
	Width: 500 nm				Helaing time: 60 min	18.3%	
Diamond single crystals nanobeam	Tensile direction: ⟨100⟩	Completely fractured	Formation of amorphous diamond osteoblasts hybridized by a mixture of sp^2 and sp^3 on the fracture surface, interatomic interaction forces change from repulsion to attraction, C–C re-bonding	Room temperature without pressure, high vacuum	Healing time: 480 min	6.7%	163
	Tensile direction: ⟨110⟩				Healing time: 60 min	5.1%	
	Tensile direction: ⟨111⟩				Healing time: 480 min	5.6%	
Single crystal SiC nanowires	Diameter: 87 nm	Completely fractured	Re-bonding and self-matching of stack faults	Room temperature, high vacuum	Healing time: 20 min	12.9%	164
Amorphous SiC nanowires	Diameter: 102 nm	Completely fractured	Re-bonding of Si–C and Si–Si bonds, atomic diffusion	Room temperature, high vacuum	Healing time: 2 s	63.6%	164,165
SiC with amorphous and crystalline composite structures nanowires	Diameter: 187 nm	Completely fractured	Re-bonding of Si–C, C–C and Si–Si bonds, atomic migration	Room temperature, high vacuum	Healing time: 20 min	11.7%	166
Si with crystalline-amorphous composite structures nanowires	Diameter: 59 nm	Completely fractured	Spontaneous re-bonding, atomic rearrangement, and van der Waals attraction	Room temperature, high vacuum	Healing time: 20 min	10.1%	167
Ti_3AlC_2 nanowires	Diameter: 93 nm	Completely fractured	The cleavage behavior, atomic migrations, and re-bonding on fracture surfaces	Room temperature, high vacuum	Healing time: 1 min	27.6%	168
					Healing time: 5 min	36.2%	
2D Graphene		Plasma-induced damage	Atom migration and adatom-vacancy recombination	Plasma irradiation		Slower Damage at Grain Boundaries	169
SiBCN blocks		The cracks prepared using Vickers indentation	High-temperature oxidation generates liquid-like products to fill the crack	High temperature (1000 °C) air atmosphere		Cracks are eliminated	168,170
Polycrystalline Al_2O_3 blocks		Deep surface cracks	The growth of grains	High temperature (1700 °C) heat treatment for 1 hour		Cracks are eliminated	171
Spinel ($MgAl_2O_4$) ceramic		Pre-cracked	Abnormal grain growth and sintering phenomena	High temperature (1600 °C) heat treatment for 1 hour, air atmosphere		91%	172

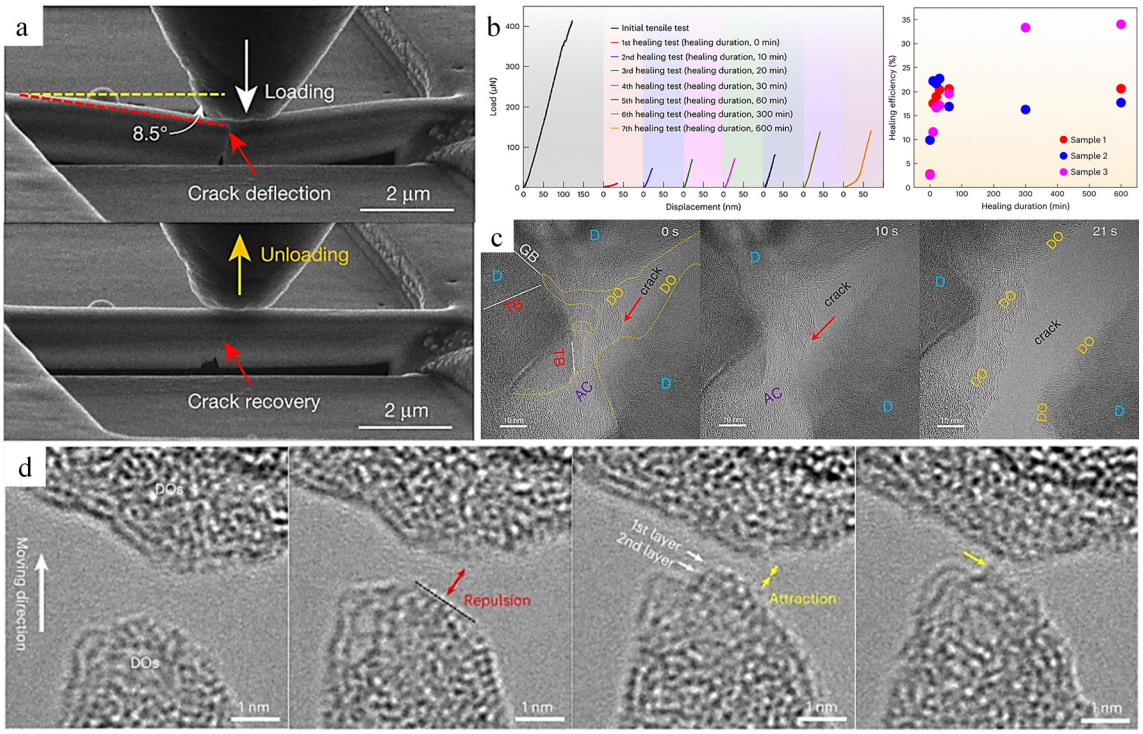

Fig. 11 Study of the self-healing behaviour of ntDC. (a) The SENB test of ntDC.[149] Reproduced with permission from ref. 149, Copyright 2020, Springer Nature. (b) Testing of mechanical properties with different healing times of ntDC. (c) DOs formation process. (d) Atomic-scale healing processes of ntDC.[163] Reproduced with permission from ref. 163, Copyright 2023, Springer Nature.

sp^3 hybridized carbon which is named "Diamond Osteocytes" (DOs). It plays a crucial role in the self-healing process of the diamond and is the key factor for achieving self-healing. When fractures with DOs phases are close to each other, the interatomic interactions first show repulsive forces, and with further proximity to reach a critical distance the repulsive forces are changed to attractive forces, followed by the formation of new C–C bonds to achieve self-healing (Fig. 11d). This repulsive force is attributed to the fact that after the fracture of diamond, approximately half of the carbon atoms on the cracked surface undergo a transformation from sp^3 hybridization to sp^2 hybridization, and the half-occupied p_z orbitals protruding outward from the surface form dangling bonds. Moreover, due to the insulating properties of diamond, charges accumulate on the surface of the fracture, thereby giving rise to the repulsive effect. When a critical distance is reached, it causes a sharp decrease in energy, thus changing from repulsive to attractive force. Benefiting from the advantages of the hierarchical structure of ntDC, such as diamond polytypes, nanotwins, stacking faults, *etc.*, a large number of DOs can be generated at the fracture surface of ntDC, and these DOs promote the self-healing behavior. In addition, even the ntDC with width ~500 nm showed room temperature self-healing ability, but the maximum healing efficiency was only 18.3%, which also indicates that the maximum healing efficiency is closely related to the cross-sectional size of the sample. This also explains why no room-temperature self-healing behavior was observed for diamond at the macroscopic size. Similarly, single crystal diamond exhibits a similar self-healing phenomenon. However, because only a small amount of DO forms on the diamond fracture surface, and the material at the fracture site disintegrates as a result of brittle fracture, the effective contact area is significantly reduced. As a result, the healing efficiency, which is approximately 6.7%, is much lower compared to that of nanocrystalline diamond (ntDC).

Interestingly, even though the fracture surface was covered with amorphous DOs, Qiu *et al.* found no atomic diffusion behavior during the healing process.[163] And DOs showed significant flexibility in tracing the atomic bonding self-healing process (Fig. 12a–f). Moreover, through first principles calculations, they further revealed the significance of amorphous DOs for the self-healing of diamond. The maximum repulsive force that needs to be overcome when two 3C diamond (111) facets are close to each other is about 12.82 GPa (Fig. 12g), whereas the maximum repulsive force that needs to be overcome when a DOs enriched with 34.7% of sp^3 hybridized carbon is close to each other is only 5.73 GPa (Fig. 12h).[163] This is due to the fact that the sp^2 bonds in the DOs on the fracture surface can greatly increase the electrical conductivity, thereby reducing the charge accumulation on the surface, which effectively reduces the repulsive force and promotes the self-healing process. The relationship between the content of sp^3 hybridized carbon in DOs and the maximum repulsive force also shows that the higher the content of sp^3 bonding, the greater the maximum repulsive force (Fig. 12i), and the repulsive force also reaches a maximum of about 12.82 GPa when the sp^3 content reaches 100%.

Zeng *et al.* investigated the toughening and crack healing mechanism of diamond by molecular dynamics simulations.[173]

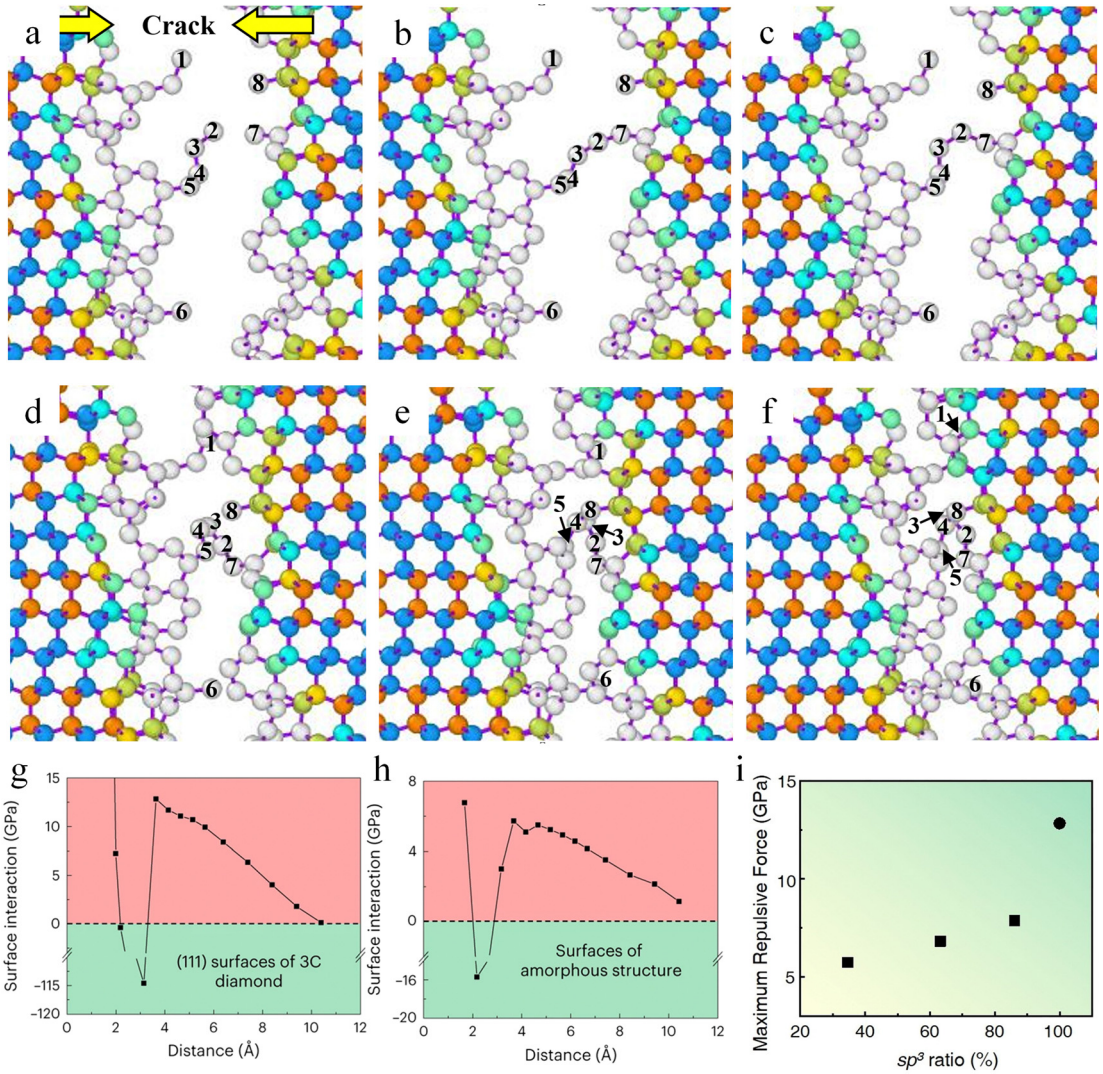

Fig. 12 Simulation of the self-healing process between two fractured ends of ntDC. (a)–(f) Molecular dynamics simulation of the ntDC crack healing process with DOs. (g) Force per area *versus* distance curve between two (111) surfaces of diamond. (h) Force per area *versus* distance curve between two amorphous DO structures with an sp^3 ratio of 34.7%. (i) The maximum repulsive force per area *versus* sp^3 content.[163] Reproduced with permission from ref. 163, Copyright 2023, Springer Nature.

During the fracture processes of diamond single crystals, nanotwinned diamond, and 2H diamond polytypes, researchers have observed that the fracture surface of diamond single crystals is extremely flat and smooth (Fig. 13a). The fracture surface of nanotwinned diamond shows randomly distributed atomic clusters (Fig. 13b), while the fracture surface of 2H diamond polytypes exhibits an even larger number of disordered atomic clusters (Fig. 13c). These disordered atomic clusters can effectively impede crack propagation, thus significantly enhancing the fracture toughness of diamond materials. For diamond samples subjected to tensile fracture, once the applied load is removed, if the fracture surface exhibits exceptional smoothness, the fractured edges can align with remarkable precision, facilitating an almost flawless self-healing response (Fig. 13d–f). However, once there are disordered atomic clusters on the fracture surface, these atomic clusters will act as obstacles, making it difficult for the carbon atoms on the fracture surfaces to re-combine precisely and perfectly, thus severely affecting the degree of self-healing (Fig. 13g–i). Zeng *et al.* pointed out that the crack healing occurs during unloading, and its extent is associated with whether the fracture surfaces are clean.[173] And a similar phenomenon occurs in 9R diamonds.

Doping boron into diamond can transform it into p-type semiconductors suitable for microelectronics and photonic devices; however, the short and strong C–C bonds complicate the doping process. Ion implantation is one way of doping, but high-energy boron ions in the MeV range can cause damage to the diamond lattice.[174] As detected by Raman spectroscopy, the one-phonon peak broadens and shifts to lower frequencies with a structured and intense background, indicating diamond lattice damage.[174,175] Agulló-Rueda *et al.* found that after annealing at 1000 °C for 1 h, the position and width of the one-phonon peak were tilted towards the original values, while the background

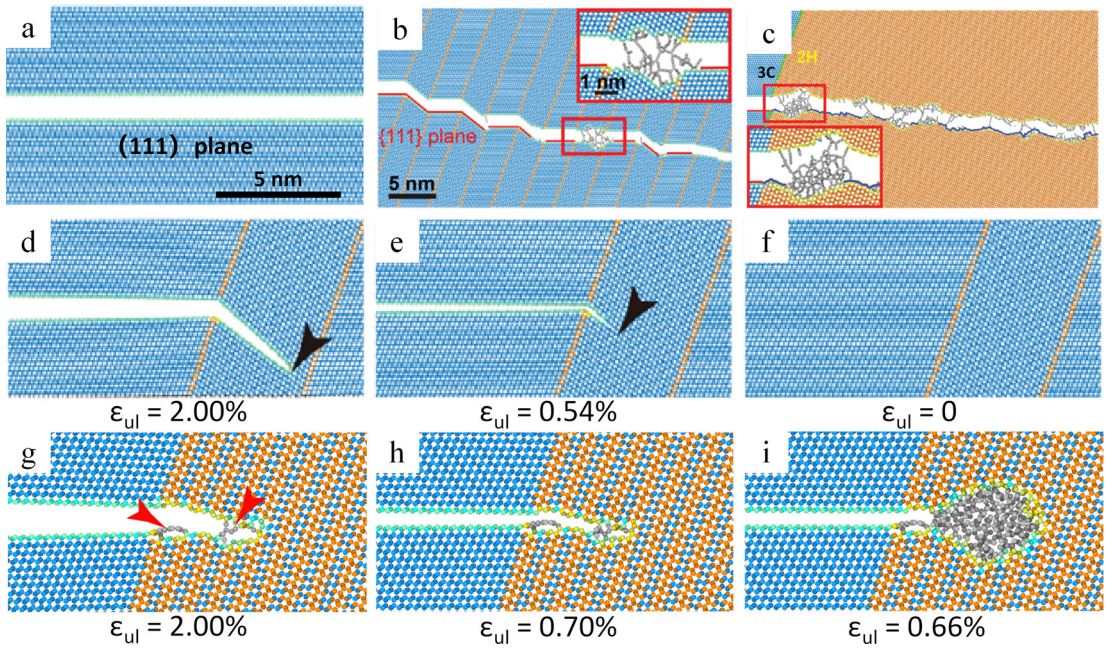

Fig. 13 Theoretical study of self-healing behavior of diamonds. (a)–(c) Crack propagation path in diamond single crystal, nanotwinned diamond and 2H diamond. (d)–(f) Crack healing in nanotwinned diamond. (g)–(i) Crack healing in 4H diamond.[173] Reproduced with permission from ref. 173, Copyright 2021, American Physical Society.

almost disappeared, indicating a partial recovery of the damaged diamond lattice.[174] Further, Jiménez-Riobóo *et al.* found that carbon atoms are displaced from the boron atom injection path and location, eventually forming amorphous/crystalline hybridized regions.[176] The Raman spectroscopic examination shows that the damaged area was repaired after vacuum annealing at 1000 °C (Fig. 14a). The recovery of the diamond lattice is achieved by the injection path of the C interstitial from the neighboring region to B and thermally activated diffusion at the B position. In addition, annealing at 1200 °C is detrimental to the diamond

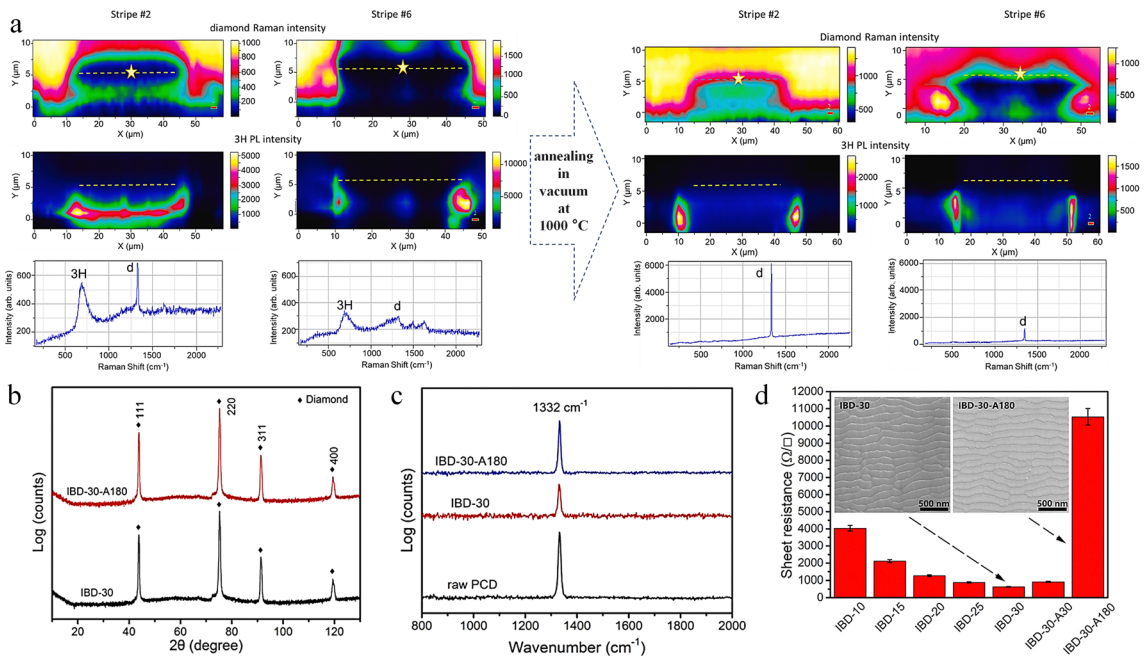

Fig. 14 Annealing to repair diamond surface damage. (a) Repair of B-ion implantation-induced damage by annealing in vacuum at 1000 °C.[176] Reproduced with permission from ref. 176, Copyright 2023, Elsevier. (b) X-ray diffraction spectrum of PCD before and after 30 keV Ar ion bombardment. (c) Raman spectra before and after the annealing in vacuum (5.0 Pa) at 1200 °C for 180 min. (d) The sheet resistance of the PCD.[177] Reproduced with permission from ref. 177, Copyright 2021, Elsevier.

lattice and leads to traces of graphitization compared to 1000 °C. Focused ion beams of Ga ions, broad Ar ion beams, *etc.* cause damage to the structure of the diamond surface when processing diamond.[177,178] The structural damage induced by ion implantation severely reduces the intrinsic thermal conductivity of diamond. Yuan *et al.* systematically investigated the evolution of corrugated morphology and chemical composition changes on the surface of the polycrystalline chemical vapor deposition diamond (PCD) under Ar ion beam bombardment with different incidence angles, ion energies and bombardment times.[177] During ion bombardment, a large number of lattice damages or defects appeared on the PCD surface due to the conversion of sp^3 hybridized C to sp^2 hybridized C. After high temperature (1200 °C) annealing in vacuum (5.0 Pa), the physical phase did not change (Fig. 14b), while the intensity of the characteristic diamond peaks in the Raman spectra was restored, indicating that the damage was repaired (Fig. 14c), and that the resistance of the thin layer increased with annealing time under annealing conditions (Fig. 14d).

3.2.2 Self-healing of other permanent covalent bonded materials. In addition to the strong C–C bond, the self-healing behavior of other permanent covalent bond materials also depends on the re-bonding process of their own permanent covalent bond, such as the room temperature self-healing behavior of Si, SiC, *et al.*[164,166,167] Si has a crystal structure quite similar to that of diamond. However, the strength of the Si–Si bond formed between silicon atoms is significantly weaker than that of the C–C bond between carbon atoms.[179] Cui *et al.* investigated the room temperature self-healing behavior of fully fractured Si with crystalline-amorphous composite structures nanowires and found that a single crystal Si with a diameter of 59 nm showed a healing efficiency of 10.1% at room temperature (Fig. 15a).[167] According to high-resolution transmission electron microscopy (HRTEM) images before and after healing (Fig. 15b and c), the gap between the fracture surfaces became smaller or disappeared after self-healing, indicating that atomic rearrangement occurred on the fracture surface. Due to the difference in strength between the crystalline and amorphous structures, the fracture surfaces were relatively rough. After the unloading force, the distance between the two fracture surfaces could hardly reach the atomic level. The researchers pointed out that the force required for fracture after healing was much higher than the van der Waals force. Therefore, it is speculated that there are other factors promoting the self-healing of silicon nanowires. In addition, through molecular dynamics simulations and in-depth discussions, it is further revealed that when two smooth fractures are in close proximity, atoms near the center of the fracture surface experience a stronger attractive force, indicating that the stress field is uneven (Fig. 15d). When the surface energy decreases after the fracture surfaces are joined, the bonding atoms in a suspended state will spontaneously recombine to reduce their own atomic energy. A rough fracture surface can reduce the fracture strength after healing, and the rough structure on the fracture surface will induce local compressive stress after the external force is unloaded. However, this local compressive stress can be released through atomic rearrangement. During the healing process, as the fracture surfaces get closer to each other, the van der Waals attractive force increases continuously. This promotes the spontaneous recombination of atoms and dangling bonds, leading to a decrease in surface energy, atomic potential energy, nanowire potential energy, and total energy. In conclusion, spontaneous rebonding, atomic rearrangement, and van der Waals attractive force are the main factors for the self-healing of silicon nanowires. Cui *et al.* further pointed out that the self-healing behavior of single crystal silicon exhibits a distinct orientation effect.[164] Specifically, among different crystal orientations, single crystal silicon with a ⟨111⟩ orientation has the highest self-healing efficiency, followed by the ⟨100⟩ orientation, while the ⟨110⟩ orientation has the lowest self-healing efficiency. In addition, the smoothness of the single crystal silicon surface also has a significant impact on its self-healing efficiency. The smoother the surface, the higher the self-healing efficiency. In addition, if the dangling bonds created on the fractured surfaces are passivated upon exposure to air, the passivated surfaces become resistant to re-bonding, thereby diminishing the overall self-healing efficiency.

Different from non-polar covalent Si materials, polar covalent SiC exhibits different room temperature self-healing mechanisms. Zhang *et al.* investigated the self-healing behavior of SiC nanowires and revealed that single crystal SiC nanowires have a 12.9% self-healing efficiency (Fig. 15e).[164] Each fracture occurred at the same position. According to the HRTEM results, the stacking faults were mismatched before healing (Fig. 15f), while the stacking faults were self-matched after self-healing (Fig. 15g). In addition, recrystallization and re-bonding occurred in the ⟨111⟩ direction during crack healing. Molecular dynamics simulations indicate that suspended bonds on the fracture surface do not oxidize under vacuum conditions, resulting in a high energy state. To reach a stable state, the system minimizes the potential energy of the suspended bonds, with the re-bonding of Si and C being the most effective method. After inducing the amorphization of single crystal SiC by electron beam irradiation and repeating the self-healing experiment, it was found that, different from single crystal SiC, amorphous SiC consistently fractured at distinct locations with each iteration (Fig. 15h–k). This indicates that the strength after healing is higher than that of the original amorphous phase, and the healing efficiency (67%) is much higher than that of single crystal SiC. This is due to the occurrence of recrystallization and re-bonding along the ⟨111⟩ orientation, forming a new interface composed of the amorphous phase and the crystalline phase. And atomic diffusion behavior was also found in this process. Single crystal SiC exhibits relatively ordered dangling bonds. In stark contrast, amorphous SiC not only has disordered dangling bonds but also has a greater number of dangling bonds per unit area. Disordered dangling bonds enables more dynamic movement of atoms on the fracture surface of amorphous SiC. Such atomic diffusion is conducive to eliminating the mismatched Si–C bonds at the healing sites and can relocate the atoms back to their original lattice structure in the ⟨111⟩ direction. Compared with single crystal SiC, amorphous SiC can more readily achieve the re-bonding of Si–C bonds. This process is beneficial for

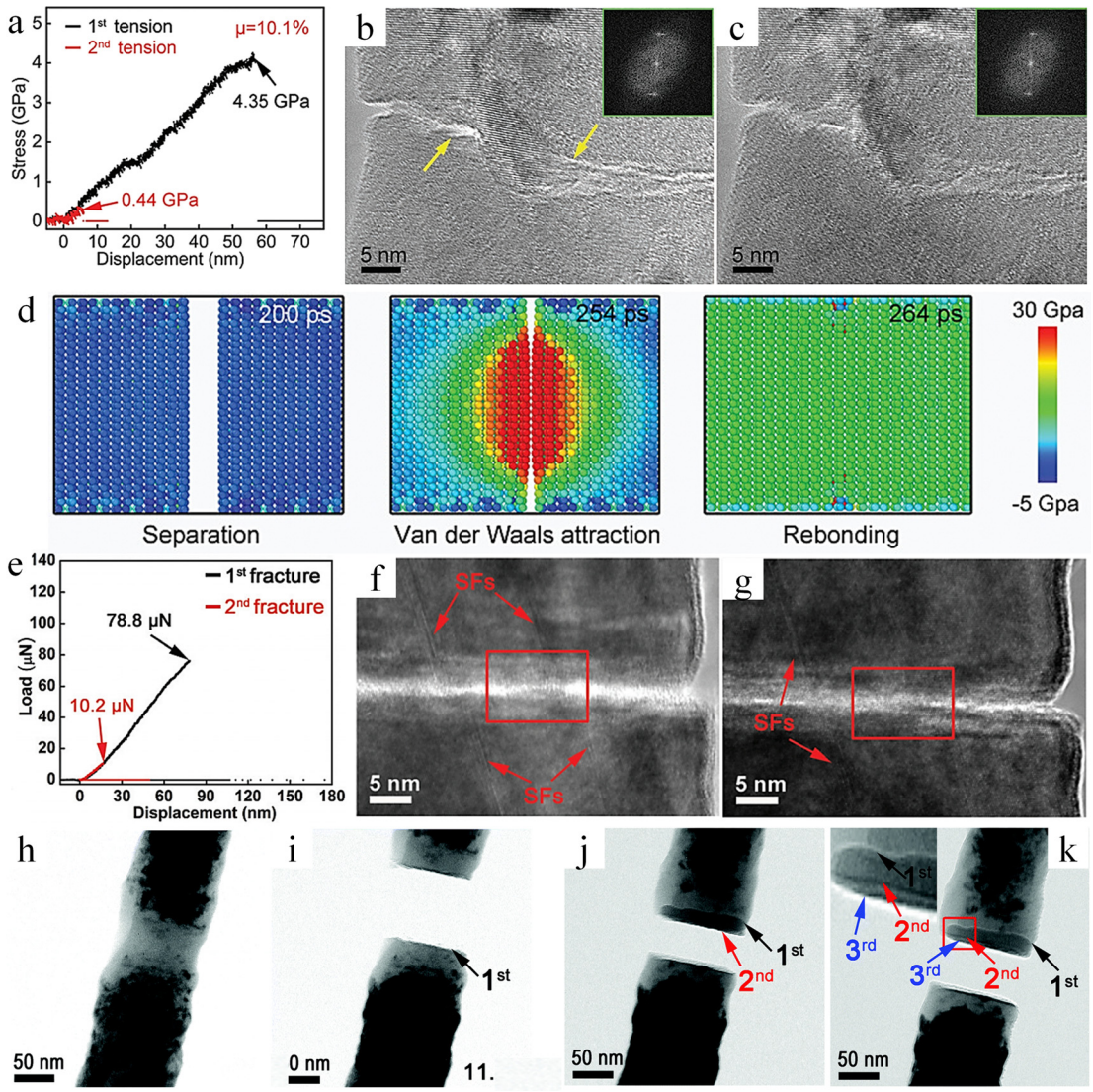

Fig. 15 Study on self-healing behavior of single crystal Si and SiC. (a) Mechanical properties of Si nanowires before and after healing. (b) and (c) The HRTEM of Si nanowires before and after healing. (d) Molecular dynamics simulation of Si nanowire self-healing.[167] Reproduced with permission from ref. 167, Copyright 2022, Wiley-VCH. (e) Mechanical properties of SiC nanowires before and after healing. (f) and (g) The HRTEM of SiC nanowires before and after healing. (h)–(k) TEM image at the fracture after multiple cycle fracture.[164] Reproduced with permission from ref. 164, Copyright 2018, Royal Society of Chemistry.

enhancing the fracture strength and elastic modulus of amorphous silicon carbide after crack healing.

Cui *et al.* also investigated the self-healing behavior of amorphous silicon carbide by *in situ* electron microscopy, and the results showed a self-healing efficiency of 63.6% (Fig. 16a).[165] The HRTEM images taken before and after self-healing revealed that the cracks had disappeared, indicating effective healing (Fig. 16b). However, unlike the previous study, both fractures broke at the same location and no crystals were formed before and after self-healing.[164] As a typical polar semiconductor, the fracture of SiC induces the generation of charges with opposite polarities on the fracture surfaces. These charges give rise to electrostatic forces, which play a pivotal role in facilitating the self-healing process of SiC nanowires.[180] These charges then form electrostatic forces, which play a crucial role in the self-healing process of SiC nanowires. In addition, the disordered overhang bonds at the amorphous SiC fracture can be directly bonded without the need to reorient the bonds like crystals, and the atomic rearrangement is conducive to the self-healing of amorphous SiC. According to the results of molecular dynamics simulation, healing is achieved by reorganization of Si–C bonds forming Si–C and Si–Si bonds (Fig. 16c and d). Subsequently, Zhang *et al.* investigated the self-healing behavior on a fractured surface of SiC with an amorphous and crystalline (AAC) composite structure.[166] Its diameter up to 187 nm can still show self-healing behavior, and the healing efficiency is about 11.7% (Fig. 16e).

Comparison of HRTEM images (Fig. 16f) before and after self-healing reveals that before self-healing, the mismatched fracture surface of the contact has a gap of 17 nm in length, and after self-healing, the mismatched fracture surface grows by

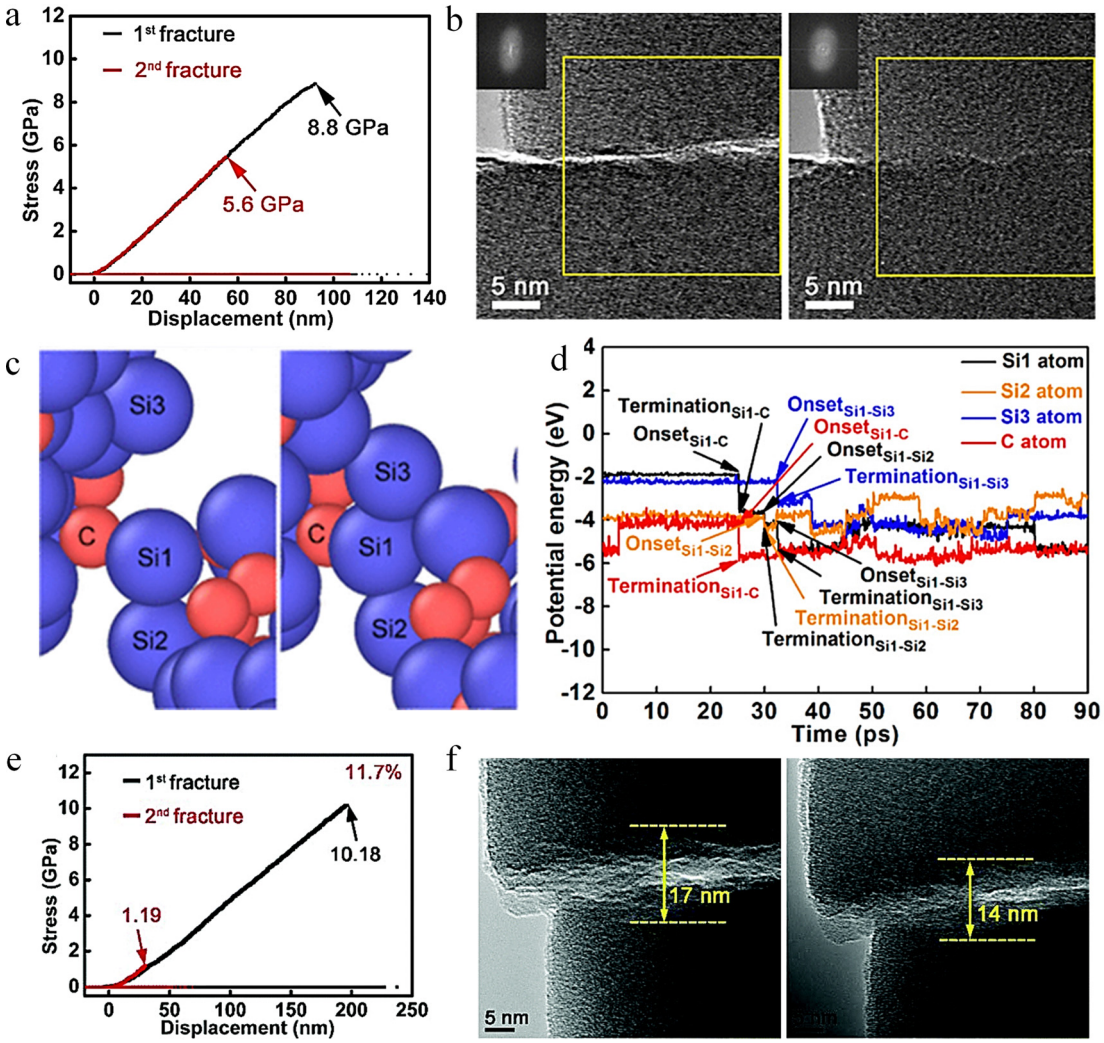

Fig. 16 Study on self-healing behavior of amorphous SiC and AAC SiC. (a) Mechanical properties of amorphous SiC nanowires before and after healing. (b) The HRTEM of amorphous SiC nanowires before and after healing. (c) and (d) Molecular dynamics simulation of amorphous SiC nanowire self-healing.[165] Reproduced with permission from ref. 165, Copyright 2019, American Chemical Society. (e) Mechanical properties of AAC SiC nanowires before and after healing. (f) The HRTEM of AAC SiC nanowires before and after healing.[166] Reproduced with permission from ref. 166, Copyright 2020, Royal Society of Chemistry.

3 nm to fill up the gap, which is reduced to 14 nm. This is inconsistent with the phenomenon for pure single crystal SiC and pure amorphous SiC.[164,165] Through molecular dynamics simulation, it is pointed out that the potential energy is reduced by re-bonding, while the potential energy is increased by debonding. The re-bonding of the C–Si, C–C and Si–Si pairs of atoms reduces the potential energy, respectively. Through coherent re-bonding and de-bonding, the potential energy of C–Si and Si–Si atoms is reduced respectively. Different from the self-healing mechanism of pure crystal and pure amorphous SiC, the healing process of AAC SiC achieves atomic migration through coherent re-bonding and debonding, thus filling the gap.

Unlike superhard/hard covalent bonding materials such as SiC, Si, and diamond, the MAX phase is a ternary compound due to the covalent bonding of M–X and the metal bonding of M–A.[181] The Ti_3AlC_2 MAX phase is used as an example, where Ti–C is covalently bonded and Ti–Al is metallically bonded. Ti_3AlC_2 nanowires exhibit high room temperature self-healing efficiency, which can reach 36.2% when the diameter is 93 nm (Fig. 17a), and the maximum healing efficiency also exhibits a size dependence, with the larger the size, the lower the healing efficiency.[168] After 1 min of self-healing in the fractured sample, the cracks on the fractured surface healed and atomic recombination was observed (Fig. 17b). Due to the lower cleavage energy of the Ti–Al bond compared to the Ti–C bond, fracture predominantly occurs along the Ti–Al interface, resulting in a smoother fracture surface and consequently enhancing the self-healing efficiency. Molecular dynamics simulation results indicate that initially, Al atoms on the opposing fracture surfaces form Al–Al bonds. This formation allows the nanowires to bear tensile stress. As the fracture surfaces continue to move closer, Al atoms re-bond with Ti atoms to form Al–Ti bonds, thereby releasing the tensile stress. This leads to a decrease in the

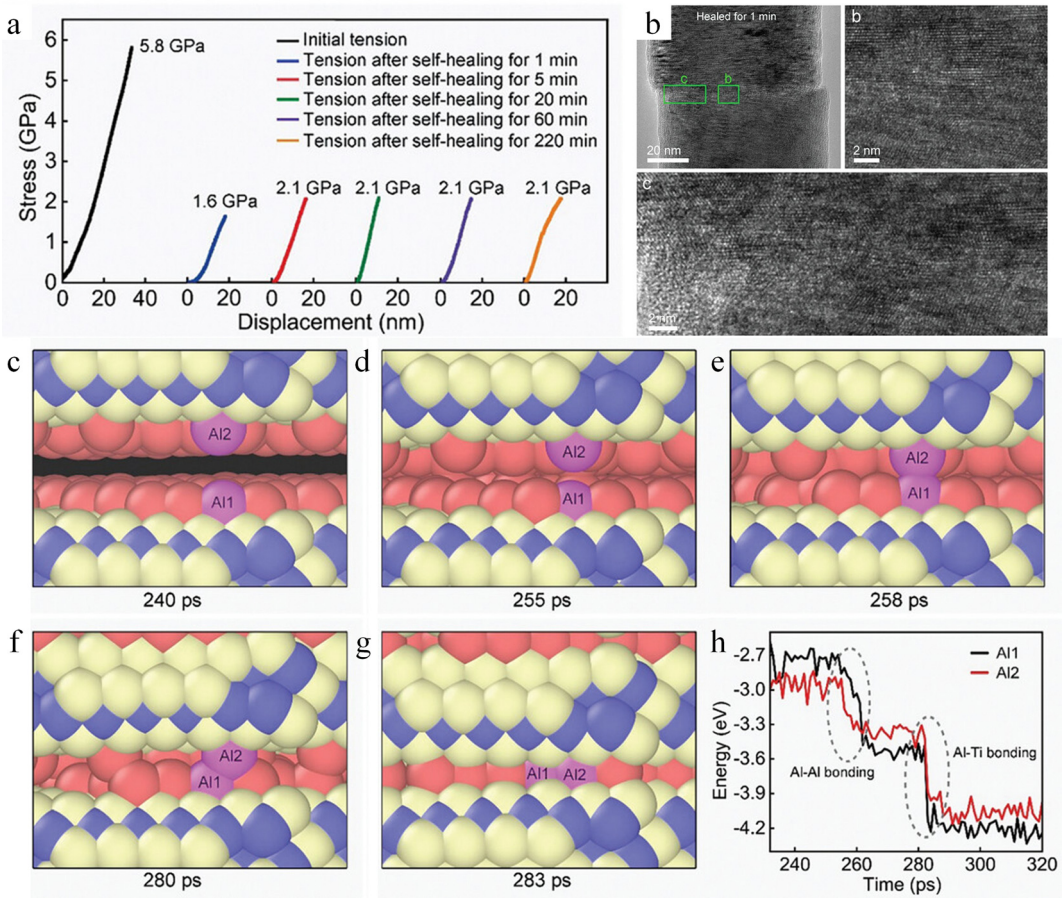

Fig. 17 Study of the self-healing behavior of Ti_3AlC_2 MAX phase. (a) Stress–displacement curves obtained from healing experiments. (b) Characterization of fracture surfaces of Ti_3AlC_2. (c)–(h) The self-healing process between two fracture surfaces of the Ti_3AlC_2.[168] Reproduced with permission from ref. 168, Copyright 2024, Wiley-VCH.

potential energy and total energy of the nanowires, driving the self-healing process forward. During the healing process, surface relaxation is the primary factor affecting the self-healing efficiency. This is because after surface relaxation, some Al atoms move to the region between Al and Ti, impeding the direct bonding between Al and Ti. However, the atomic migration of Al atoms can effectively counteract the adverse effects caused by surface relaxation (Fig. 17c–h). Throughout the healing process, the Ti–C covalent bond did not directly participate in the breaking and re-bonding of chemical bonds.

3.2.3 Influencing factors of self-healing. In macroscopic superhard material samples, the strength recovered after healing is often extremely weak compared to the initial strength of the sample, almost negligible. This makes it extremely difficult to accurately detect the recovery of the material's mechanical properties at this scale. Due to the above-mentioned reasons, in the field of superhard materials, it has long been generally believed that achieving self-healing is nearly an impossible task. However, research results in recent years have successfully broken this traditional concept. Currently, research on the self-healing characteristics of superhard covalent bond materials mainly focuses on the micro- and nanoscale ranges. It is worth noting that as the size of the materials gradually increases, their healing efficiency shows a continuous downward trend. Besides, there are other factors influencing their healing efficiency. In this regard, we have made the following summary:

1. Size effect: a strong and significant correlation exists between the healing efficiency of superhard and covalently bonded materials and the size of the samples. Generally speaking, the smaller the sample size, the higher the healing efficiency. This is mainly due to the fact that as the size decreases, the surface energy of the material increases accordingly. As a result, after fracture, the material is more likely to recombine to reduce the total potential energy of the system. In addition, the smaller the size, the smoother the fracture surface of the material, which undoubtedly creates favorable conditions for the self-healing process.

2. Degree of fracture mismatch: when two fractured surfaces approach each other, there is a substantial likelihood of experiencing relative misalignment during their contact. The impact of this phenomenon cannot be underestimated. It not only reduces the effective contact area, thereby leading to a decrease in strength and misassessment of stress, but also hinders the process of crystal-oriented bonding. The greater the degree of misalignment of the fractured surfaces, the lower the healing efficiency of the material.

3. Roughness of fracture surface: the research results indicate that the smoother and cleaner the fractured surfaces are, the higher the healing efficiency will be. When the fractured surfaces are rough, cavities will form during the closure of the fracture, leading to stress concentration in some areas. Such rough surfaces not only reduce the effective contact area but also prolong the healing time.

4. Healing time and healing frequency: healing time is a prerequisite for the self-healing of materials. When the self-healing process involves the re-formation of chemical bonds, extending the healing time is of vital importance. This can not only enable more chemical bonds to re-bond but also guarantee the high quality of these re-formed bonds, thus providing a solid foundation for the recovery of the material's properties. Meanwhile, sufficient time is also essential for the atomic diffusion process. An adequate amount of time ensures that the atomic diffusion occurs fully and perfectly, allowing atoms to migrate to appropriate positions and further facilitating the repair of the material's internal structure. Within the maximum achievable healing efficiency range of the material, there is an obvious positive correlation between the healing time and the healing efficiency. That is, the longer the healing time, the higher the healing efficiency. Research results on the self-healing behavior of diamond show that the healing frequency plays a crucial role in the self-healing performance of diamond. Increasing the healing frequency can promote the formation of DOs, which in turn drives a significant increase in the healing efficiency. Therefore, for those healing mechanisms involving the evolution of surface structure, the influence of healing frequency must be fully considered in practical research and application.

5. Degree of amorphization: current research results indicate that the amorphous structure, characterized by its disordered nature, offers significant advantages in terms of re-bonding. When a material undergoes an amorphization transformation, this change may potentially promote the self-healing behavior of the material. However, it is important to note that the amorphization process may also bring about some negative effects. One of these is the reduction in the surface cleanliness of the material, which in turn affects the fitting state of the fractured surfaces and ultimately leads to a decrease in the healing efficiency.

6. Environmental factors: the environment is crucial for a material's self-healing. Temperature, pressure, and oxygen content are key factors. Higher temperatures aid atomic diffusion by providing atoms with more energy to overcome lattice barriers, facilitating post-fracture re-bonding. However, excessive heat can cause thermal damage, altering the material's internal structure and impairing its performance and self-healing ability; pressure also matters. Appropriate pressure brings fractured surfaces closer, increasing atomic interaction and potentially enhancing bonding efficiency and the self-healing process; oxygen can also significantly impact self-healing. In an oxygen environment, dangling bonds on the fractured surface oxidize. Oxidation reduces their activity and the material's potential energy, making atomic re-bonding harder and hindering self-healing.

Research on self-healing superhard covalently bonded materials is still in its infancy. There may be a variety of potential factors in addition to those mentioned above. For example, the microstructural design of the material itself, as well as other factors that have not yet been identified. All these aspects urgently require more in-depth research. Especially at the atomic scale, in-depth dissection of the micro-mechanisms of self-healing is essential to further improve the healing efficiency of materials.

4. Conclusion and outlook

Currently, research on self-healing materials is being carried out vigorously in various fields. The concept of self-healing materials emerged as a significant innovative idea in the field of materials science. Its core objective is to endow materials with the function of autonomously repairing damage, thereby prolonging the service life of materials and enhancing their reliability. Among a wide variety of self-healing materials, new self-healing superhard covalent-bonded materials have stood out and attracted much attention. The unique covalent bonding in superhard covalently bonded materials endows them with a range of excellent mechanical properties, including very high hardness, excellent wear resistance, and strong strength, but also poses challenges for the design and development of self-healing superhard covalently bonded materials. Currently, the research on self-healing superhard covalent bonding materials is still in the early exploration stage. The covalent bonding system itself is extremely complex, and how to strike a delicate balance between maintaining superhard properties and realizing self-healing capability poses a great challenge to research efforts.

This paper systematically and comprehensively reviews the extrinsic self-healing mechanisms, such as microencapsulation embedment, oxidative healing mechanism, and shape memory assisted healing, as well as the intrinsic self-healing mechanisms including dynamic covalent bonds, supramolecular interactions, diffusive behavior, and defect-driven processes. It elaborates on how these extrinsic and intrinsic healing mechanisms inspire the design of self-healing superhard covalently bonded materials. Meanwhile, it focuses on reviewing the research status of the self-healing behavior of superhard covalently bonded materials, deeply analyzes the key factors affecting their self-healing efficiency, aiming to assist researchers in better understanding and designing novel self-healing superhard covalently bonded materials.

For the study of the self-healing behavior of superhard covalent bonding materials, especially how to design and prepare superhard covalent bonding materials with high healing efficiency, the following key challenges must be addressed and overcome: (a) at present, a comprehensive and systematic theoretical model is lacking. This model should fully cover various influencing factors such as the type of inter atomic bonding, bond length/bond energy, crystal structure, grain size, dislocation density, *etc.* Through quantitative analysis, an accurate relationship between hardness and theoretical self-healing

ability should be established, and then a practical theoretical guidance framework can be formed. (b) It is necessary to vigorously promote the continuous innovation of advanced characterization techniques, especially to focus on the development of direct bonding techniques for permanent covalent bonds. This not only plays a decisive role in the precise design of self-healing superhard covalent bond materials but also has equally important significance for the innovative development of wafer direct bonding technology. (c) When developing new self-healing superhard covalent bond materials, on the one hand, it is necessary to carefully design their microstructure at the micro-nano scale to ensure the maintenance of high hardness while significantly improving the comprehensive performance. On the other hand, starting from the atomic scale, chemical bonds should be precisely regulated to achieve high efficiency self-healing. (d) Achieving high precision positioning healing of the fracture surface, greatly improving the healing efficiency, and realizing controllable and rapid healing of permanent covalent bonds are crucial factors in overcoming the bottlenecks that hinder the practical application of materials. (e) Currently, the research on the self-healing behavior of superhard covalent bond materials mainly relies on transmission electron microscopes in a high vacuum environment to conduct analysis from the atomic scale. However, achieving reliable self-healing under complex working conditions (such as extreme conditions like high temperature, low temperature, high pressure, radiation, oxygen atmosphere, *etc.*) is the core and key to realizing the wide range practical application of this material. The development of self-healing superhard covalently bonded materials will have important potential applications in a number of industrial fields such as cutting tools, aerospace, electronics, *etc.* This progress could pave the way for the emergence of numerous innovative technologies in the near future, offering substantial benefits across various sectors.

Author contributions

K. Q., X. L. contributed equally to this work. Y. Y., L. G., proposed and supervised the project; K. Q., X. L., Y. L., Y. Y., L. G. wrote the review together.

Data availability

No primary research results, software or code have been included and no new data were generated or analysed as part of this review.

Conflicts of interest

There are no conflicts to declare.

Acknowledgements

This work was supported by grants from the National Key R&D Program of China (2024YFA1209800), the National Natural Science Foundation of China (U23A20542, 52494930, 51972009, 51922017) and the State Key Laboratory of Silicate Materials for Architectures (Wuhan University of Technology) (SYSJJ2024-03).

References

1 M. Li, A. R. Mao, Q. W. Guan and E. Saiz, *Chem. Soc. Rev.*, 2024, **53**, 8240–8305.
2 Y. Liu, B. Chen, Z. Liu, Z. Zhang and R. O. Ritchie, *Prog. Mater. Sci.*, 2024, **144**, 101281.
3 S. Zhao and J. H. Ahn, *Mater. Sci. Eng., R*, 2022, **148**, 100672.
4 D. Nepal, S. Kang, K. M. Adstedt, K. Kanhaiya, M. R. Bockstaller, L. C. Brinson, M. J. Buehler, P. V. Coveney, K. Dayal, J. A. El-Awady, L. C. Henderson, D. L. Kaplan, S. Keten, N. A. Kotov, G. C. Schatz, S. Vignolini, F. Vollrath, Y. Wang, B. I. Yakobson, V. V. Tsukruk and H. Heinz, *Nat. Mater.*, 2022, **22**, 18–35.
5 S. An, B. Shi, M. Jiang, B. Fu, C. Song, P. Tao, W. Shang and T. Deng, *Chem. Rev.*, 2023, **123**, 7081–7118.
6 U. H. Kim, E. J. Lee, C. S. Yoon, S. T. Myung and Y. K. Sun, *Adv. Energy Mater.*, 2016, **6**, 1601417.
7 H. A. Bale, A. Haboub, A. A. MacDowell, J. R. Nasiatka, D. Y. Parkinson, B. N. Cox, D. B. Marshall and R. O. Ritchie, *Nat. Mater.*, 2012, **12**, 40–46.
8 S. Lavenstein, Y. J. Gu, D. Madisetti and J. A. El-Awady, *Science*, 2020, **370**, 190.
9 G. Gao, F. Yang, F. Zhou, J. He, W. Lu, P. Xiao, H. Yan, C. Pan, T. Chen and Z. L. Wang, *Adv. Mater.*, 2020, **32**, 2004290.
10 F. Awaja, S. Zhang, M. Tripathi, A. Nikiforov and N. Pugno, *Prog. Mater. Sci.*, 2016, **83**, 536–573.
11 Y. Cao, Y. J. Tan, S. Li, W. W. Lee, H. Guo, Y. Cai, C. Wang and B. C. K. Tee, *Nat. Electron.*, 2019, **2**, 75–82.
12 S. Bonardd, M. Nandi, J. I. Hernández García, B. Maiti, A. Abramov and D. Díaz Díaz, *Chem. Rev.*, 2022, **123**, 736–810.
13 A. Zarepour, S. Ahmadi, N. Rabiee, A. Zarrabi and S. Iravani, *Nano-Micro Lett.*, 2023, **15**, 100.
14 J. Kang, J. B. H. Tok and Z. Bao, *Nat. Electron.*, 2019, **2**, 144–150.
15 I. L. Hia, V. Vahedi and P. Pasbakhsh, *Polym. Rev.*, 2016, **56**, 225–261.
16 S. Wang and M. W. Urban, *Nat. Rev. Mater.*, 2020, **5**, 562–583.
17 P. Greil, *J. Adv. Ceram.*, 2013, **1**, 249–267.
18 S. Zhang, N. van Dijk and S. van der Zwaag, *Acta Metall. Sin.*, 2020, **33**, 1167–1179.
19 D. G. Bekas, K. Tsirka, D. Baltzis and A. S. Paipetis, *Composites, Part B*, 2016, **87**, 92–119.
20 J. W. C. Pang and I. P. Bond, *Compos. Sci. Technol.*, 2005, **65**, 1791–1799.
21 S. K. Ghosh, *Self-Healing Materials*, 2008, pp. 1–28, DOI: 10.1002/9783527625376.ch1.
22 S. Bhunia, S. Chandel, S. K. Karan, S. Dey, A. Tiwari, S. Das, N. Kumar, R. Chowdhury, S. Mondal, I. Ghosh, A. Mondal, B. B. Khatua, N. Ghosh and C. M. Reddy, *Science*, 2021, **373**, 321–327.

23 J. Cui, Y. Bao, Q. Dai, F. Li, H. Wang, Y. Liu, F. Cao and J. Li, *Adv. Funct. Mater.*, 2024, 2405737, DOI: **10.1002/adfm.202405737**.
24 J. Xu, J. Chen, Y. Zhang, T. Liu and J. Fu, *Angew. Chem., Int. Ed.*, 2021, **60**, 7947–7955.
25 S. Zhang, Y. H. Cheng, L. Galuska, A. Roy, M. Lorenz, B. Chen, S. Luo, Y. T. Li, C. C. Hung, Z. Qian, P. B. J. St. Onge, G. T. Mason, L. Cowen, D. Zhou, S. I. Nazarenko, R. F. Storey, B. C. Schroeder, S. Rondeau-Gagné, Y. C. Chiu and X. Gu, *Adv. Funct. Mater.*, 2020, **30**, 2000663.
26 Y. Yao, Z. Xu, B. Liu, M. Xiao, J. Yang and W. Liu, *Adv. Funct. Mater.*, 2020, **31**, 2006944.
27 E. Z. Alharissa, N. Nashrah, R. A. K. Putri, W. Al Zoubi and Y. G. Ko, *Adv. Compos. Hybrid Mater.*, 2024, **7**, 16.
28 C. Ye, D. Liu, X. Peng, Y. Jiang, R. Cheng, C. Ning, F. Sheng, Y. Zhang, K. Dong and Z. L. Wang, *ACS Nano*, 2021, **15**, 18172–18181.
29 J. Liu, Z. Tong, F. Gao, J. Wang, J. Hu, L. Song, Y. Hou, J. Lu, X. Zhan and Q. Zhang, *Adv. Mater.*, 2024, **36**, 2401982.
30 Y. M. Li, Z. P. Zhang, M. Z. Rong and M. Q. Zhang, *Adv. Mater.*, 2023, **35**, 2211009.
31 R. B. Leonesio, *J. Am. Ceram. Soc.*, 2006, **55**, 437–439.
32 G. L. Gaines and D. Tabor, *Nature*, 1956, **178**, 1304–1305.
33 Y. M. Malinskii, V. V. Prokopenko, N. A. Ivanova and V. A. Kargin, *Polym. Mech.*, 1973, **6**, 240–244.
34 Y. M. Malinskii, V. V. Prokopenko, N. A. Ivanova and V. S. Kargin, *Polym. Mech.*, 1973, **6**, 382–384.
35 Y. M. Malinskii, V. V. Prokopenko and V. A. Kargin, *Polym. Mech.*, 1973, **6**, 969–972.
36 R. J. Gray, *Cem. Concr. Res.*, 1984, **14**, 315–317.
37 S. R. White, N. R. Sottos, P. H. Geubelle, J. S. Moore, M. R. Kessler, S. R. Sriram, E. N. Brown and S. Viswanathan, *Nature*, 2001, **409**, 794–797.
38 G. Williams, R. Trask and I. Bond, *Composites, Part A*, 2007, **38**, 1525–1532.
39 K. S. Toohey, C. J. Hansen, J. A. Lewis, S. R. White and N. R. Sottos, *Adv. Funct. Mater.*, 2009, **19**, 1399–1405.
40 B. Aizenshtein and L. Etgar, *Small*, 2023, **20**, 2305755.
41 C. O. W. Trost, A. Lassnig, P. Kreiml, T. Jörg, V. L. Terziyska, C. Mitterer and M. J. Cordill, *Adv. Mater.*, 2024, **36**, 2401007.
42 A. K. Padhan, D. Sharma, T. S. Thomas, A. P. Sinha, A. N. Mallick and D. Mandal, *J. Mater. Chem. A*, 2024, **12**, 9508–9517.
43 J. Wang, J. Tang, D. Chen, S. Xing, X. Liu and J. Hao, *Polym. Compos.*, 2023, **44**, 6304–6323.
44 V. L. Solozhenko and E. Gregoryanz, *Mater. Today*, 2005, **8**, 44–51.
45 Z. Zhang and J. Brgoch, *J. Am. Chem. Soc.*, 2022, **144**, 18075–18080.
46 B. Xu and Y. Tian, *Sci. China: Mater.*, 2015, **58**, 132–142.
47 Y. Tian, B. Xu and Z. Zhao, *Int. J. Refract. Met. Hard Mater.*, 2012, **33**, 93–106.
48 R. B. Kaner, J. J. Gilman and S. H. Tolbert, *Science*, 2005, **308**, 1268–1269.
49 P. Ying, B. Z. Li, M. D. Ma, Y. F. Gao, R. X. Sun, Z. H. Li, S. Chen, B. Zhang, H. F. Li, B. Liu, L. Sun, S. Zhao, K. Tong, W. T. Hu, Y. L. Pan, G. D. Tang, D. L. Yu, Z. S. Zhao, B. Xu and Y. J. Tian, *Nat. Synth.*, 2025, **4**, 391–398.
50 Y. Tian, B. Xu, D. Yu, Y. Ma, Y. Wang, Y. Jiang, W. Hu, C. Tang, Y. Gao, K. Luo, Z. Zhao, L.-M. Wang, B. Wen, J. He and Z. Liu, *Nature*, 2013, **493**, 385–388.
51 R. X. Sun, X. D. Wei, W. T. Hu, P. Ying, Y. J. Wu, L. Y. Wang, S. Chen, X. Zhang, M. D. Ma, D. L. Yu, L. Wang, G. Y. Gao, B. Xu and Y. J. Tian, *Small*, 2022, **18**, 2201212.
52 Z. Zhao, B. Xu and Y. Tian, *Annu. Rev. Mater. Res.*, 2016, **46**, 383–406.
53 K. S. Toohey, N. R. Sottos, J. A. Lewis, J. S. Moore and S. R. White, *Nat. Mater.*, 2007, **6**, 581–585.
54 S. Meure, D. Y. Wu and S. Furman, *Acta Mater.*, 2009, **57**, 4312–4320.
55 S. Gupta, Q. Zhang, T. Emrick, A. C. Balazs and T. P. Russell, *Nat. Mater.*, 2006, **5**, 229–233.
56 J. Wang, M. Wu, J. Huang, Y. Wang, X. Miao, Y. Chen, D. Bian and Y. Zhao, *ACS Appl. Mater. Interfaces*, 2024, **16**, 26768–26786.
57 J. Martínez Lucci, R. S. Amano and P. K. Rohatgi, *Heat Mass Transfer*, 2016, **53**, 825–848.
58 K. K. Alaneme and M. O. Bodunrin, *Appl. Mater. Today*, 2017, **6**, 9–15.
59 J.-J. Chen, H. Xie, L.-Z. Liu, H. Guan, Z. You, L. Zou and H.-J. Jin, *Science*, 2024, **385**, 629–633.
60 X. Lu, S. Li, W. Zhang, B. Yao, W. Yu and Y. Zhou, *J. Eur. Ceram. Soc.*, 2019, **39**, 4023–4028.
61 K. Takahashi, M. Yokouchi, S. K. Lee and K. Ando, *J. Am. Ceram. Soc.*, 2004, **86**, 2143–2147.
62 S. Li, L. Xiao, G. Song, X. Wu, W. G. Sloof, S. van der Zwaag and Y. Zhou, *J. Am. Ceram. Soc.*, 2013, **96**, 892–899.
63 Y. Liu, H. Liu, C. Huang, L. Ji, L. Wang, Y. Yuan, Q. Liu and Q. Han, *Ceram. Int.*, 2023, **49**, 13790–13798.
64 J. Lin, Y. Huang and H. Zhang, *Ceram. Int.*, 2014, **40**, 16811–16815.
65 G. M. Song, Y. T. Pei, W. G. Sloof, S. B. Li, J. T. M. De Hosson and S. van der Zwaag, *Scr. Mater.*, 2008, **58**, 13–16.
66 B. Yao, S. Li, W. Zhang, W. Yu, Y. Zhou, S. Fan and G. Bei, *J. Adv. Ceram.*, 2022, **11**, 1687–1695.
67 S. Li, L. Zhang, W. Yu and Y. Zhou, *Ceram. Int.*, 2017, **43**, 6963–6966.
68 W.-C. Kim, K.-R. Lim, W.-T. Kim, E.-S. Park and D.-H. Kim, *Prog. Mater. Sci.*, 2022, **123**, 100756.
69 J. B. Ferguson, B. F. Schultz and P. K. Rohatgi, *Mater. Sci. Eng., A*, 2015, **620**, 85–88.
70 P. K. Rohatgi, *Mater. Sci. Eng., A*, 2014, **619**, 73–76.
71 N. Salowitz, S. Misra, M. I. Haider, M. Povolo and P. Rohatgi, *Materials*, 2022, **15**, 2970.
72 E. L. Kirkby, J. D. Rule, V. J. Michaud, N. R. Sottos, S. R. White and J. A. E. Månson, *Adv. Funct. Mater.*, 2008, **18**, 2253–2260.
73 J. Champagne, S.-S. Pang and G. Li, *Composites, Part B*, 2016, **97**, 344–352.
74 Y. Shi, C. B. Cooper, T. Nogusa, J.-C. Lai, H. Lyu, M. Khatib, C. Xu, L. Michalek and Z. Bao, *Matter*, 2024, **7**, 2108–2124.
75 C. R. Fisher, H. B. Henderson, M. S. Kesler, P. Zhu, G. E. Bean, M. C. Wright, J. A. Newman, L. C. Brinson,

O. Figueroa and M. V. Manuel, *Appl. Mater. Today*, 2018, **13**, 64–68.
76 C. C. Hornat and M. W. Urban, *Nat. Commun.*, 2020, **11**, 1028.
77 S. Samanta, S. Kim, T. Saito and A. P. Sokolov, *J. Phys. Chem. B*, 2021, **125**, 9389–9401.
78 M. Burnworth, L. Tang, J. R. Kumpfer, A. J. Duncan, F. L. Beyer, G. L. Fiore, S. J. Rowan and C. Weder, *Nature*, 2011, **472**, 334–337.
79 H. Ying, Y. Zhang and J. Cheng, *Nat. Commun.*, 2014, **5**, 3218.
80 X. Liu, Y. Li, X. Fang, Z. Zhang, S. Li and J. Sun, *ACS Mater. Lett.*, 2022, **4**, 554–571.
81 X. Chen, M. A. Dam, K. Ono, A. Mal, H. Shen, S. R. Nutt, K. Sheran and F. Wudl, *Science*, 2002, **295**, 1698–1702.
82 K. P. Faseela, A. P. Benny, Y. Kim and S. Baik, *Small*, 2021, **18**, 2104764.
83 T. Wang, W.-W. Kong, W.-C. Yu, J.-F. Gao, K. Dai, D.-X. Yan and Z.-M. Li, *Nano-Micro Lett.*, 2021, **13**, 162.
84 Y. Lai, X. Kuang, P. Zhu, M. Huang, X. Dong and D. Wang, *Adv. Mater.*, 2018, **30**, 1802556.
85 J. Ma, Y. Yang, C. Valenzuela, X. Zhang, L. Wang and W. Feng, *Angew. Chem., Int. Ed.*, 2022, **61**, e202116219.
86 J. Canadell, H. Goossens and B. Klumperman, *Macromolecules*, 2011, **44**, 2536–2541.
87 G. P. Carden, M. L. Martins, G. Toleutay, S. Ge, B. Li, S. Zhao and A. P. Sokolov, *Macromolecules*, 2024, **57**, 8621–8631.
88 S. Cho, S. Y. Hwang, D. X. Oh and J. Park, *J. Mater. Chem. A*, 2021, **9**, 14630–14655.
89 M. Irigoyen, A. Fernández, A. Ruiz, F. Ruipérez and J. M. Matxain, *J. Org. Chem.*, 2019, **84**, 4200–4210.
90 X. Zhang and R. M. Waymouth, *J. Am. Chem. Soc.*, 2017, **139**, 3822–3833.
91 S. P. Black, J. K. M. Sanders and A. R. Stefankiewicz, *Chem. Soc. Rev.*, 2014, **43**, 1861–1872.
92 H. Otsuka, S. Nagano, Y. Kobashi, T. Maeda and A. Takahara, *Chem. Commun.*, 2010, **46**, 1150–1152.
93 A. Ruiz de Luzuriaga, R. Martin, N. Markaide, A. Rekondo, G. Cabañero, J. Rodríguez and I. Odriozola, *Mater. Horiz.*, 2016, **3**, 241–247.
94 Y. Amamoto, H. Otsuka, A. Takahara and K. Matyjaszewski, *Adv. Mater.*, 2012, **24**, 3975–3980.
95 O. R. Cromwell, J. Chung and Z. Guan, *J. Am. Chem. Soc.*, 2015, **137**, 6492–6495.
96 M. O. Saed, A. Gablier and E. M. Terentejv, *Adv. Funct. Mater.*, 2019, **30**, 1906458.
97 Y. Yuan, Y. Sun, S. Yan, J. Zhao, S. Liu, M. Zhang, X. Zheng and L. Jia, *Nat. Commun.*, 2017, **8**, 14657.
98 H. Memon, H. Liu, M. A. Rashid, L. Chen, Q. Jiang, L. Zhang, Y. Wei, W. Liu and Y. Qiu, *Macromolecules*, 2020, **53**, 621–630.
99 S. Zhao and M. M. Abu-Omar, *Macromolecules*, 2018, **51**, 9816–9824.
100 S. Bhattacharya, R. S. Phatake, S. Nabha Barnea, N. Zerby, J.-J. Zhu, R. Shikler, N. G. Lemcoff and R. Jelinek, *ACS Nano*, 2019, **13**, 1433–1442.
101 D. Zhao, M. Feng, L. Zhang, B. He, X. Chen and J. Sun, *Carbohydr. Polym.*, 2021, **256**, 117580.
102 H. Feng, T. Wang, W. Wang, C. Ma, Y. Pu and S. Chen, *J. Mater. Sci. Technol.*, 2024, **173**, 121–136.
103 Y. Wang, M. Yang and Z. Zhao, *Carbohydr. Polym.*, 2023, **310**, 120723.
104 J.-H. Gao, B. Wan, M.-S. Zheng, L. Luo, H. Zhang, Q.-L. Zhao, G. Chen and J.-W. Zha, *Mater. Horiz.*, 2024, **11**, 1305–1314.
105 C. Zhang, M. Wang, C. Jiang, P. Zhu, B. Sun, Q. Gao, C. Gao and R. Liu, *Nano Energy*, 2022, **95**, 106991.
106 B. Zhou, D. He, J. Hu, Y. Ye, H. Peng, X. Zhou, X. Xie and Z. Xue, *J. Mater. Chem. A*, 2018, **6**, 11725–11733.
107 L. Wang, Z. L. Gong, S. Y. Li, W. Hong, Y. W. Zhong, D. Wang and L. J. Wan, *Angew. Chem., Int. Ed.*, 2016, **55**, 12393–12397.
108 J. Chen, Y. Gao, L. Shi, W. Yu, Z. Sun, Y. Zhou, S. Liu, H. Mao, D. Zhang, T. Lu, Q. Chen, D. Yu and S. Ding, *Nat. Commun.*, 2022, **13**, 4868.
109 Y. Jia, Q. Guan, C. Chu, L. Zhang, R. E. Neisiany, S. Gu, J. Sun and Z. You, *Sci. Bull.*, 2024, **69**, 1875–1886.
110 Y. Liu, X. Chen, S. Yin, X. Chang, C. Lv, J. Zang, X. Leng, T. Zhang and G. Zhao, *ACS Nano*, 2022, **16**, 19472–19481.
111 Z. Wang, J. Fan, D. He, L. Ren, Z. Hao, R. Sun and X. Zeng, *J. Mater. Chem. A*, 2022, **10**, 21923–21932.
112 X. Zhu, W. Zhang, G. Lu, H. Zhao and L. Wang, *ACS Nano*, 2022, **16**, 16724–16735.
113 R. Han, F. Zeng, Q. Xia, X. Pang and X. Wu, *Carbohydr. Polym.*, 2024, **340**, 122271.
114 Y. Han, K. Zhao, G. Chen, R. A. Li, C. Zhou, Z. Hua, H. Duan and M. He, *J. Mater. Chem. A*, 2023, **11**, 19637–19644.
115 J. Xu, Y. Li, T. Liu, D. Wang, F. Sun, P. Hu, L. Wang, J. Chen, X. Wang, B. Yao and J. Fu, *Adv. Mater.*, 2023, **35**, 2300937.
116 J.-B. Hou, X.-Q. Zhang, D. Wu, J.-F. Feng, D. Ke, B.-J. Li and S. Zhang, *ACS Appl. Mater. Interfaces*, 2019, **11**, 12105–12113.
117 M. Mohamadhoseini and Z. Mohamadnia, *Coord. Chem. Rev.*, 2021, **432**, 213711.
118 L. Xiao, W. Xu, L. Huang, J. Liu and G. Yang, *Adv. Compos. Hybrid Mater.*, 2022, **6**, 15.
119 F. Mo, Q. Li, G. Liang, Y. Zhao, D. Wang, Y. Huang, J. Wei and C. Zhi, *Adv. Sci.*, 2021, **8**, 2100072.
120 H. Lv, X. Chu, Y. Zhang, Q. Liu, F. Wu and D. Mu, *Mater. Today*, 2024, **78**, 181–208.
121 E. B. Stukalin, L.-H. Cai, N. A. Kumar, L. Leibler and M. Rubinstein, *Macromolecules*, 2013, **46**, 7525–7541.
122 L. N. Neumann, E. Oveisi, A. Petzold, R. W. Style, T. Thurn-Albrecht, C. Weder and S. Schrettl, *Sci. Adv.*, 2021, **7**, eabe4154.
123 Y. H. Kim and R. P. Wool, *Macromolecules*, 2002, **16**, 1115–1120.
124 M. D. Hager, P. Greil, C. Leyens, S. van der Zwaag and U. S. Schubert, *Adv. Mater.*, 2010, **22**, 5424–5430.
125 C. Chen, W. B. Ying, J. Li, Z. Kong, F. Li, H. Hu, Y. Tian, D. H. Kim, R. Zhang and J. Zhu, *Adv. Funct. Mater.*, 2021, **32**, 2106341.

126 J. M. Azpiroz, E. Mosconi, J. Bisquert and F. De Angelis, *Energy Environ. Sci.*, 2015, **8**, 2118–2127.
127 B. P. Finkenauer, Akriti, K. Ma and L. Dou, *ACS Appl. Mater. Interfaces*, 2022, **14**, 24073–24088.
128 Y. Cheng, X. Liu, Z. Guan, M. Li, Z. Zeng, H. W. Li, S. W. Tsang, A. G. Aberle and F. Lin, *Adv. Mater.*, 2020, **33**, 2006170.
129 Y. Rakita, I. Lubomirsky and D. Cahen, *Mater. Horiz.*, 2019, **6**, 1297–1305.
130 Y. Rakita, S. R. Cohen, N. K. Kedem, G. Hodes and D. Cahen, *MRS Commun.*, 2015, **5**, 623–629.
131 M. B. Al-Handawi, G. Dushaq, P. Commins, D. P. Karothu, M. Rasras, L. Catalano and P. Naumov, *Adv. Mater.*, 2022, **34**, 2109374.
132 S. K. Yadavalli, Z. Dai, H. Zhou, Y. Zhou and N. P. Padture, *Acta Mater.*, 2020, **187**, 112–121.
133 B. P. Finkenauer, Y. Gao, X. Wang, Y. Tian, Z. Wei, C. Zhu, D. J. Rokke, L. Jin, L. Meng, Y. Yang, L. Huang, K. Zhao and L. Dou, *Cell Rep. Phys. Sci.*, 2021, **2**, 100320.
134 B. Wang, Y. Han, S. Xu, L. Qiu, F. Ding, J. Lou and Y. Lu, *Small*, 2018, **14**, 1704085.
135 G. S. Ferguson, M. K. Chaudhury, G. B. Sigal and G. M. Whitesides, *Science*, 1991, **253**, 776–778.
136 D. V. Wagle and G. A. Baker, *Mater. Horiz.*, 2015, **2**, 157–167.
137 S. Zhang, C. Kwakernaak, W. Sloof, E. Brück, S. van der Zwaag and N. van Dijk, *Adv. Eng. Mater.*, 2015, **17**, 598–603.
138 R. N. Lumley, A. J. Morton and I. J. Polmear, *Acta Mater.*, 2002, **50**, 3597–3608.
139 O. Kovalenko, C. Brandl, L. Klinger and E. Rabkin, *Adv. Sci.*, 2017, **4**, 1700159.
140 C. Chen, S. Nagao, K. Suganuma, J. Jiu, H. Zhang, T. Sugahara, T. Iwashige, K. Sugiura and K. Tsuruta, *Appl. Phys. Lett.*, 2016, **109**, 093503.
141 R. Xin, Q. Ma and W. Li, *Mater. Sci. Eng., A*, 2016, **662**, 65–71.
142 J. Zang, Z.-H. Xu, R. A. Webb and X. Li, *Nano Lett.*, 2010, **11**, 241–244.
143 C. M. Barr, T. Duong, D. C. Bufford, Z. Milne, A. Molkeri, N. M. Heckman, D. P. Adams, A. Srivastava, K. Hattar, M. J. Demkowicz and B. L. Boyce, *Nature*, 2023, **620**, 552–556.
144 T. Irifune, A. Kurio, S. Sakamoto, T. Inoue and H. Sumiya, *Nature*, 2003, **421**, 599–600.
145 Q. Huang, D. Yu, B. Xu, W. Hu, Y. Ma, Y. Wang, Z. Zhao, B. Wen, J. He, Z. Liu and Y. Tian, *Nature*, 2014, **510**, 250–253.
146 S. Zhang, Z. Li, K. Luo, J. He, Y. Gao, A. V. Soldatov, V. Benavides, K. Shi, A. Nie, B. Zhang, W. Hu, M. Ma, Y. Liu, B. Wen, G. Gao, B. Liu, Y. Zhang, Y. Shu, D. Yu, X.-F. Zhou, Z. Zhao, B. Xu, L. Su, G. Yang, O. P. Chernogorova and Y. Tian, *Natl. Sci. Rev.*, 2022, **9**, nwab140.
147 H. Tang, X. Yuan, Y. Cheng, H. Fei, F. Liu, T. Liang, Z. Zeng, T. Ishii, M.-S. Wang, T. Katsura, H. Sheng and H. Gou, *Nature*, 2021, **599**, 605–610.
148 Y. Shang, Z. Liu, J. Dong, M. Yao, Z. Yang, Q. Li, C. Zhai, F. Shen, X. Hou, L. Wang, N. Zhang, W. Zhang, R. Fu, J. Ji, X. Zhang, H. Lin, Y. Fei, B. Sundqvist, W. Wang and B. Liu, *Nature*, 2021, **599**, 599–604.
149 Y. Yue, Y. Gao, W. Hu, B. Xu, J. Wang, X. Zhang, Q. Zhang, Y. Wang, B. Ge, Z. Yang, Z. Li, P. Ying, X. Liu, D. Yu, B. Wei, Z. Wang, X.-F. Zhou, L. Guo and Y. Tian, *Nature*, 2020, **582**, 370–374.
150 X. Zhao, X. He, Y. Sun, J. Yi and P. Xiao, *Acta Mater.*, 2009, **57**, 893–902.
151 D. Laniel, F. Trybel, A. Aslandukov, S. Khandarkhaeva, T. Fedotenko, Y. Yin, N. Miyajima, F. Tasnádi, A. V. Ponomareva, N. Jena, F. I. Akbar, B. Winkler, A. Néri, S. Chariton, V. Prakapenka, V. Milman, W. Schnick, A. N. Rudenko, M. I. Katsnelson, I. A. Abrikosov, L. Dubrovinsky and N. Dubrovinskaia, *Adv. Mater.*, 2023, **36**, 2308030.
152 A. Mansouri Tehrani, A. O. Oliynyk, M. Parry, Z. Rizvi, S. Couper, F. Lin, L. Miyagi, T. D. Sparks and J. Brgoch, *J. Am. Chem. Soc.*, 2018, **140**, 9844–9853.
153 A. L. Ivanovskii, *Prog. Mater. Sci.*, 2012, **57**, 184–228.
154 Y. L. Pan, P. Ying, Y. F. Gao, P. Liu, K. Tong, D. L. Yu, K. L. Jiang, W. T. Hu, B. Z. Li, B. Liu, Z. S. Zhao, J. L. He, B. Xu, Z. Y. Liu and Y. J. Tian, *Proc. Natl. Acad. Sci. U. S. A.*, 2021, **118**, e2108340118.
155 X. L. He, X. Dong, Q. S. Wu, Z. S. Zhao, Q. Zhu, A. R. Oganov, Y. J. Tian, D. L. Yu, X. F. Zhou and H. T. Wang, *Phys. Rev. B*, 2018, **97**, 100102(R).
156 P. Jacobson and S. Stoupin, *Diamond Relat. Mater.*, 2019, **97**, 107469.
157 X. M. Sun, D. Y. Cong, Y. Ren, D. E. Brown, R. G. Li, S. H. Li, Z. Yang, W. X. Xiong, Z. H. Nie, L. Wang and Y. D. Wang, *Appl. Phys. Lett.*, 2018, **113**, 041903.
158 S. Liu, L. Han, Y. Zou, P. Zhu and B. Liu, *J. Mater. Sci. Technol.*, 2017, **33**, 1386–1391.
159 R. Sun, X. Zhang, X. Hao, W. Hu, X. Wei, X. Song, Z. Zhang, P. Ying, S. Zhao, Y. Wang, Y. Gao, D. Yu, B. Xu, G. Gao and Y. Tian, *J. Eur. Ceram. Soc.*, 2025, **45**, 116829.
160 E. Kulik, N. Nishiyama, Y. Higo, N. A. Gaida and T. Katsura, *J. Am. Ceram. Soc.*, 2018, **102**, 2251–2256.
161 F. M. Gao, J. L. He, E. D. Wu, S. M. Liu, D. L. Yu, D. C. Li, S. Y. Zhang and Y. J. Tian, *Phys. Rev. Lett.*, 2003, **91**, 015502.
162 Z. Zeng, J. Wen, H. Lou, X. Zhang, L. Yang, L. Tan, B. Cheng, X. Zuo, W. Yang, W. L. Mao, H.-K. Mao and Q. Zeng, *Nature*, 2022, **608**, 513–517.
163 K. Qiu, J. Hou, S. Chen, X. Li, Y. Yue, B. Xu, Q. Hu, L. Liu, Z. Yang, A. Nie, Y. Gao, T. Jin, J. Wang, Y. Li, Y. Wang, Y. Tian and L. Guo, *Nat. Mater.*, 2023, **22**, 1317–1323.
164 Z. Zhang, J. Cui, B. Wang, H. Jiang, G. Chen, J. Yu, C. Lin, C. Tang, A. Hartmaier, J. Zhang, J. Luo, A. Rosenkranz, N. Jiang and D. Guo, *Nanoscale*, 2018, **10**, 6261–6269.
165 J. Cui, Z. Zhang, H. Jiang, D. Liu, L. Zou, X. Guo, Y. Lu, I. P. Parkin and D. Guo, *ACS Nano*, 2019, **13**, 7483–7492.
166 Z. Zhang, D. Liu, F. Huo, S. Huang, J. Cui, Y. Lu, I. P. Parkin and D. Guo, *Nanoscale*, 2020, **12**, 19617–19627.
167 J. Cui, Y. Sun, H. Chen, Y. Yang, G. Chen, P. Ke, K. Nishimura, Y. Yang, C. Tang and N. Jiang, *Adv. Funct. Mater.*, 2023, **33**, 2210053.
168 J. Cui, X. Hu, L. Zhang, Y. Yang, Y. Li, G. Chen, C. Tang and P. Ke, *Adv. Funct. Mater.*, 2024, 2422697.

169 P. Vinchon, X. Glad, G. Robert Bigras, R. Martel and L. Stafford, *Nat. Mater.*, 2020, **20**, 49–54.
170 F. Liu, J. Kong, C. Luo, F. Ye, X. Luan, N. Tian, Y. Liu, H. Zhang, J. Gu and Y. Tang, *Adv. Compos. Hybrid Mater.*, 2018, **1**, 506–517.
171 F. F. Lange and K. C. Radford, *J. Am. Ceram. Soc.*, 1970, **53**, 420–421.
172 F. Tavangarian and G. Li, *Mater. Sci. Eng., A*, 2015, **641**, 201–209.
173 Y. P. Zeng, Q. Zhang, Y. J. Wang, J. X. Jiang, H. Z. Xing and X. Y. Li, *Phys. Rev. Lett.*, 2021, **127**, 066101.
174 F. Agulló-Rueda, M. D. Ynsa, N. Gordillo, A. Maira, D. Moreno-Cerrada and M. A. Ramos, *Diamond Relat. Mater.*, 2017, **72**, 94–98.
175 J. O. Orwa, K. W. Nugent, D. N. Jamieson and S. Prawer, *Phys. Rev. B: Condens. Matter Mater. Phys.*, 2000, **62**, 5461–5472.
176 R. J. Jiménez-Rioboó, N. Gordillo, A. de Andrés, A. Redondo-Cubero, M. Moratalla, M. A. Ramos and M. D. Ynsa, *Carbon*, 2023, **208**, 421–431.
177 Y. Yuan, W. Yang, J. Sang, J. Zhu, L. Fu, D. Li and L. Zhou, *Diamond Relat. Mater.*, 2021, **120**, 108670.
178 S. Kunuku, K. J. Sankaran, C.-Y. Tsai, W.-H. Chang, N.-H. Tai, K.-C. Leou and I. N. Lin, *ACS Appl. Mater. Interfaces*, 2013, **5**, 7439–7449.
179 T. Çagin, J. Che, M. N. Gardos, A. Fijany and W. A. Goddard, *Nanotechnology*, 1999, **10**, 278–284.
180 R. Madar, *Nature*, 2004, **430**, 974–975.
181 H. Ding, Y. Li, M. Li, K. Chen, K. Liang, G. Chen, J. Lu, J. Palisaitis, P. O. Å. Persson, P. Eklund, L. Hultman, S. Du, Z. Chai, Y. Gogotsi and Q. Huang, *Science*, 2023, **379**, 1130–1135.

